

# Effect of neutron irradiation on tensile properties of advanced Cu-based alloys and composites developed for fusion applications

Dmitry Terentyev<sup>a,\*</sup>, Michael Rieth<sup>b</sup>, Gerald Pintsuk<sup>c</sup>, Alexander Von Müller<sup>d</sup>, Steffen Antusch<sup>b</sup>, Aleksandr Zinovev<sup>a</sup>, Alexander Bakaev<sup>a</sup>, Kateryna Poleshchuk<sup>a,e</sup>, Giacomo Aiello<sup>f</sup>

<sup>a</sup> Belgian Nuclear Research Centre, SCK CEN, Mol 2400, Belgium

<sup>b</sup> Karlsruhe Institut für Technologie, Hermann-von-Helmholtz-Platz 1, Eggenstein-Leopoldshafen 76344, Germany

<sup>c</sup> Forschungszentrum Jülich GmbH, Institut für Energie- und Klimaforschung – Plasmaphysik, Jülich 52425, Germany

<sup>d</sup> Max-Planck-Institut für Plasmaphysik, Garching 85748, Germany

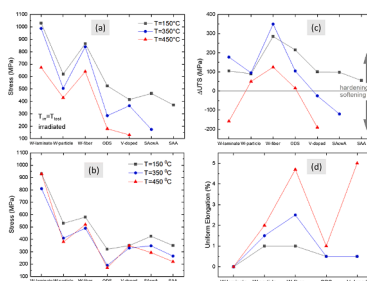
<sup>e</sup> Department of Materials, Textiles and Chemical Engineering, Ghent University (UGent), Technologiepark 903, Ghent B-9052, Belgium

<sup>f</sup> EUROfusion PMU, Boltzmannstraße 2, Garching 85749, Germany

## HIGHLIGHTS

- Neutron irradiation embrittles W-CuCrZr laminates.
- Fiber reinforced CuCrZr sustains ductility and high strength after neutron irradiation.
- Vanadium-doped and ODS alloyed materials soften under 450 °C irradiation.

## GRAPHICAL ABSTRACT



## ARTICLE INFO

**Keywords:**  
Copper  
Irradiation  
Alloys  
Composites

## ABSTRACT

The effect of neutron irradiation on tensile properties and fracture mode has been investigated for several advanced CuCrZr alloys in the frame of the European fusion material development program. Five material grades utilizing different strengthening principles have been exposed to neutron irradiation up to ~2.5 dpa (displacement per atom) in the target operational temperature range of 150–450 °C. The strengthening mechanisms are based on the application of: i) tungsten particles; ii) tungsten foils (laminar structure); iii) tungsten fibers; iv) Y<sub>2</sub>O<sub>3</sub> particles; v) vanadium addition (0.22%). Neutron irradiation was performed in the BR2 material test reactor inside the fuel channel in order to maximize the fast neutron flux. The upper irradiation temperature of 450 °C was selected to validate the ability of the pre-selected advanced grades to sustain the high temperature irradiation, since the baseline ITER specification CuCrZr is known not to retain sufficient tensile strength above 400 °C in non-irradiated conditions and shows strong irradiation induced softening above 300 °C. Neutron irradiation at 150 °C caused severe embrittlement of tungsten-copper laminates as well as a considerable reduction of the total elongation of all other grades. The irradiation at 450 °C led to the reduction of the yield strength and ultimate tensile strength (i.e. irradiation softening) in the vanadium-doped alloy similar to CuCrZr,

\* Corresponding author.

E-mail address: [dterenty@sckcen.be](mailto:dterenty@sckcen.be) (D. Terentyev).

while all other materials preserved or increased their strength (irradiation hardening). The fracture surfaces of the tested samples were analysed to investigate the modification of the deformation mechanisms in each particular case.

## 1. Introduction

Assessment of the neutron irradiation effect on thermo-mechanical properties of materials constituting the plasma-facing components (PFC) for the divertor of DEMO, a demonstration reactor and the next step towards commercial use of nuclear fusion is an important milestone on the roadmap of the European fusion material program [1]. The baseline concept of the PFC components for DEMO is similar to the one selected for ITER, which uses tungsten monoblocks with a pipe made of copper-based alloy [2–5]. The divertor PFC of ITER and DEMO will be exposed to high heat flux loads during normal operation where the temperature from the heat sink to coolant interface to the top surface of the plasma facing material will vary from 150 °C to 1200 °C (for thermal loads of up to 15 MW/m<sup>2</sup>) [6]. Following ITER requirements, the satisfactory performance of those alloys is confirmed up to an operational temperature of 300–350 °C and an irradiation dose of 0.5 dpa (displacement per atom) [7]. Above this threshold, a significant decrease of the strength is observed. However, higher neutron and thermal loads are envisaged in the PFCs of the DEMO divertor compared to ITER (i.e. neutron load ITER: 0.37–0.47, DEMO 1.8–2.4 [MW/m<sup>2</sup>], i.e. CuCrZr can reach up to 14 dpa in DEMO) [8,9]. Therefore, development of advanced heat sink materials is in line with the primary goal to expand the operational temperature window to ensure compatibility with water (i.e. operation at as low as 150 °C) and sufficient strength up to at least ~450 °C thus closing the operational temperature windows between the heat sink material and tungsten as plasma facing material. At this, the advanced Cu-based alloys are currently being developed taking CuCrZr alloy (of ITER specification) as the basis which is then improved by various means including introduction of strengthening particles, armoring wires, laminar structures or by alternation of the composition inducing other than CrZr precipitates.

Given that the matrix of the advanced Cu-based alloys is CuCrZr, it is useful to provide a brief review of its properties and irradiation effects, while more extended description is given in Section 2. The baseline material is alloyed with chromium (0.5–1.2 wt.%) and zirconium (0.05–0.25 wt.% in EN 12,167 standard) and therefore it is usually referred to as CuCrZr. The mechanical properties of CuCrZr strongly depend on its microstructure such as grain size, precipitation size and dislocation and precipitation densities. The heat treatment is therefore applied to attenuate the mechanical properties (strength and ductility) to a required performance thanks to the formation, growth and coarsening of Cr-Zr precipitates. The design of the ITER specification CuCrZr, for the application in the divertor, accounted for the irradiation dose limited to 0.3–0.5 dpa and irradiation temperature range 100–300 °C in normal conditions, and escape up to 400 °C in the transient event [10]. In the case of DEMO application, the end-of-life irradiation dose will be varied as 3–14 dpa [11], depending on the location in the divertor, therefore the currently known information about irradiation effects is not sufficient.

Fabritsiev and Pokrovsky have studied mechanical properties and irradiation-induced microstructure of the ITER specification CuCrZr [10, 12] at 80 - 300 °C up to the irradiation dose of 2.5 dpa coming to a number of important experimental observations, namely:

- (i) under irradiation at 150–200 °C there is a drastic reduction of the uniform elongation, associated with the plastic flow localization and channel deformation [13]. The saturation of the irradiation hardening and complete loss of the uniform elongation is reached already at 0.5–1 dpa,

- (ii) the irradiation at 350 °C and above leads to the softening of the material [7], which represents an issue for mechanical stability of divertor components under exposure to thermo-mechanical fatigue loads.

Given the issues pointed out in a short review of the irradiation effects on the microstructure and mechanical properties in the ITER specification CuCrZr, the main purpose of the development of the advanced heat sink alloys is to retain the tensile strength at high irradiation temperature (to push operational temperature window up to 450 °C) and avoid embrittlement/elongation reduction at lower irradiation temperature (100 - 120 °C) without major reduction of other properties owned by the baseline material.

In this work, we investigate the mechanical properties before and after irradiation of several prospective Cu-based alloys developed within the European fusion material program [1]. Five material grades utilizing different strengthening principles have been exposed to neutron irradiation up to ~2.5 dpa in the target operational temperature range of 150–450 °C. The strengthening mechanisms are based on the application of: i) tungsten particles; ii) tungsten foils (laminar structure); iii) tungsten fibers; iv) oxide dispersion strengthening (ODS) particles; v) minor alloying with vanadium. The reference and irradiated materials were tested in uniaxial tensile mode, and the fracture surface was investigated by scanning electron microscopy (SEM). The paper is organized as follows: in Section 2 we provide information about materials including baseline CuCrZr alloy of ITER specification as well as test methods applied, in Section 3 the results and their discussion is given, and finally Conclusions are drawn in Section 5.

## 2. Experimental procedures

### 2.1. Background information on baseline CuCrZr

The specification of the mechanical properties of the copper alloy for ITER application is provided in Ref [7,14]. Cu is alloyed with chromium (0.5–1.2 wt.%) and zirconium (0.05–0.25 wt.% in EN 12,167 standard), and depending on a specific application, different types of thermo-mechanical treatments are available, namely: i) solution-annealed (SA), cold-worked (cw) and aged (A); ii) solution-annealed and aged (SAA); iii) solution-annealed and overaged (SAoverA) in non-optimal conditions (applied for large scale components for which annealing regime is difficult to adhere to).

The mechanical properties of CuCrZr strongly depend on its microstructure such as grain size, precipitation size and dislocation and precipitation densities. The microstructure is developed by thermo-mechanical treatment during the production process. The alloy in SAoverA condition is characterized by an increased size of precipitates compared to the SAA condition (~20 nm after 600 °C treatment for 4 h compared to ~2 nm for SAA). The size of the precipitates, in the case of over aging, is proportional to the heat treatment temperature and time. Also, the precipitate density decreases promptly with the overaging time. Coarsening of the precipitates in the alloy and decrease of the precipitation density usually lead to a loss of the alloy strength.

The effect of the heat treatment on the strength of the CuCrZr alloy is also rather significant. The highest tensile strength, namely an ultimate tensile strength (UTS) of ~480 MPa and yield stress (YS) of ~450 MPa at room temperature (RT) are obtained for the SA<sub>cw</sub>A condition. The SAA material has a lower strength (UTS of ~400 MPa and YS of ~280 MPa at RT) which is followed by the strength of the SA<sub>overA</sub> (UTS of ~320 MPa and YS of ~200 MPa at RT [15]), while pure annealed copper is

**Table 1**

List of materials studied in this work and brief information on the chemical composition.

Material and sample ID	Reference	Supplier and material information
CuCrZr - W laminate (73% W) Label: L	W-laminate	KIT Karlsruhe W-27%CuCrZr (wt.%); 14.6 g/cm <sup>3</sup> ; 255 W/m.K (parallel), 223 W/m.K (perpendicular) Microstructure: orientation of single rolled W-sheets parallel to tensile loading
CuCrZr - W fibers (54% W) Label: F	W-fiber	IPP Garching in collaboration with Louis Renner GmbH W - 46%CuCrZr (wt.%); 12.55 g/cm <sup>3</sup> ; 267 W/m.K (parallel), 258 W/m.K (perpendicular) Microstructure: infiltrated W-fiber fabric with main fiber orientation parallel to tensile loading - minor contribution by woven fibers in perpendicular direction
CuCrZr - W particles (70% W) Label: P	W-particle	IPP Garching in collaboration with Louis Renner GmbH W-30%CuCrZr (wt.%); 14.29 g/cm <sup>3</sup> ; 243 W/m.K Microstructure: homogeneous / isotropic;
CuCrZr - V Label: V	V-doped	KIT Karlsruhe Cu-0.922%Cr-0.041%Zr-0.221%V (wt.%); ~8.90 g/cm <sup>3</sup> ; ~300-350 W/m.K (estimate) Microstructure: homogeneous / isotropic
ODS Cu - Y <sub>2</sub> O <sub>3</sub> Label: Y	ODS	KIT Karlsruhe Cu-Y <sub>2</sub> O <sub>3</sub> (heat # C3/40-Y); ~8.90 g/cm <sup>3</sup> ; assumption: 300-350 W/m.K (value is indicative); Microstructure: homogeneous / isotropic

characterized by the lowest tensile strength among the alloys processed with the conditions listed above [7]. As reported in [7] the UTS of SACwA drops from 480 MPa at RT to 290 MPa at 500 °C; UTS of SAA reduces from 400 MPa to 200 MPa at 500 °C. Moreover, specimens in the SAA and the SA in overaged conditions show a decrease in the tensile strength with increasing the annealing time. This effect was observed at 50 °C and 300 °C test temperatures.

The ductile characteristics of the ITER CuCrZr also depend on the heat treatment. The uniform elongation of SACwA at RT is 7%, this value decreases to 1% at 300 °C and remains unchanged until 700 °C [16]. For SAA the uniform elongation is 18% for RT with a linear decline to 15% at 500 °C. For SAoverA the uniform elongation at 50 °C is 26% and 19% at 300 °C. The total elongation of SACwA at RT is 19%, this value descends to 6% at 500 °C [16]. For SAA the total elongation decreases from 26% to 20% for the same temperatures. SAoverA has total elongation of 30%

at 50 °C and 24% at 300 °C.

As was briefly specified in the introduction, the mechanical properties of the ITER specification CuCrZr in neutron irradiated state were studied by Fabritsiev and Pokrovsky in Ref. [10,12]. The irradiation temperature varied from 80 up to 300 °C and the irradiation dose up to 2.5 dpa. At low irradiation temperature (150–200 °C), the saturation of the irradiation hardening and complete loss of the uniform elongation is reached at rather low dose of 0.5–1 dpa. The drastic reduction of the uniform elongation is associated with the plastic flow localization and channel deformation [13], which is not the case at the irradiation at 300 °C. The explanation for the difference was provided thanks to an TEM study. The TEM investigation of the material irradiated at 80 and 150 °C up to 0.1 dpa revealed that dislocation loops and stacking fault tetrahedra (SFT) are the two main defects induced by the irradiation [12]. Dislocation loops should represent the main source of hardening as they keep on growing in size with increasing the irradiation dose, while SFTs are limited in size (up to about 2–3 nm) [17]. The density of SFTs is  $\sim 10^{23} m^{-3}$ , while the density of the loops is one order of magnitude lower, i.e.  $10^{22} m^{-3}$ , as reported in [12]. After irradiation at 300 °C, large dislocation loops (up to 500 nm in size) were observed, besides nano-metric defects, which was ascribed to diffusion and coalescence of the in-cascade produced loops [10].

The summary of the tensile strength including non- and irradiated materials provided in [7] shows that the UTS of SACwA CuCrZr changes from 480 to 500 MPa at RT down to 280–300 MPa at 400 °C in the non-irradiated state. In the same temperature range, the strength of the SAA CuCrZr (i.e. without cold working) is about 30–50 MPa lower, depending on the test temperature. After the irradiation (to the saturation dose), the UTS of both types of materials decreases to  $\sim 280$  MPa at 300 °C. Increasing the test temperature above 300 °C leads to a further reduction of the UTS below 200 MPa, which is considered as an important limitation.

## 2.2. Advanced Cu-based alloys

The materials investigated in this work were developed as advanced risk mitigation materials in the frame of the EUROfusion project and in particular the Work Package Materials (WP-MAT) [1]. Five different materials, three of which are composites, were included in the present study. Basic information about the chemical composition and supplier is provided in Table 1. Below, we provide a brief description of each material, while detailed information can be found in the related references:

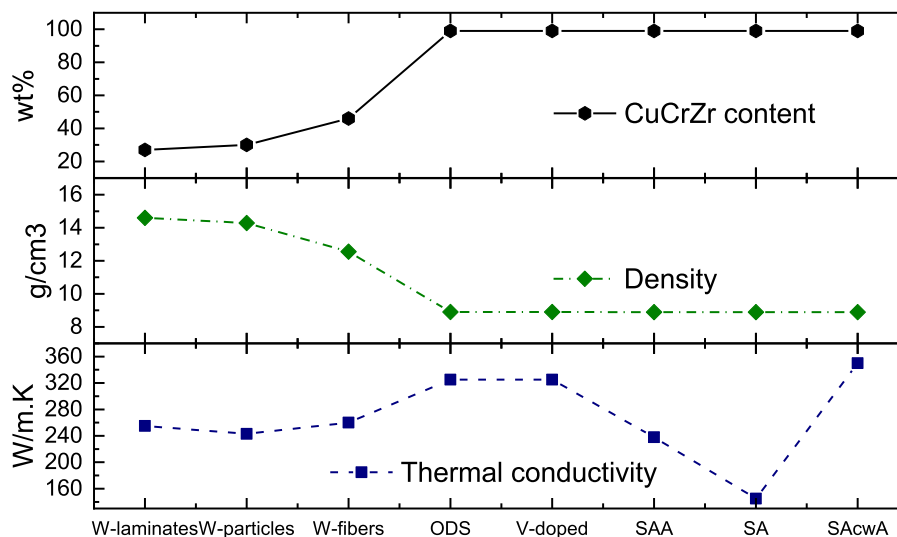


**Fig. 1.** Density and thermal conductivity measured at room temperature of the different Cu-based materials. The ODS material is based on technically pure Cu (not CuCrZr).

**Table 2**  
Irradiation conditions.

Notation used for figures	$T_{irr}$ , °C	Irradiation dose, dpa
A	150	2.15
B	350	2.5
C	450	2.55

- Tungsten – copper laminate acquires an unique combination of ductility, strength and low ductile to brittle transition temperature (DBTT) [18,19] thanks to the dedicated thermo-mechanical treatment of the W foils. CuCrZr is used as an interlayer material to bond W foils, enhance thermal conductivity and reduce irradiation induced swelling compared to using pure Cu as interlayer material. This material will be referred to as „W-laminate“.
- W fiber – copper composite [20–22] is produced for the irradiation in the form of a plate in contrast to the foreseen later use in tube shape and uses 145  $\mu\text{m}$  tungsten fibers aligned in a grid as reinforcement, while CuCrZr is infiltrated to create the bulk material. This material represents a combination of the ductile CuCrZr matrix with high-strength drawn W fibers as reinforcement. This material will be referred to as „W-fiber“.
- W particle reinforced CuCrZr containing nearly spherical W particles [23] owns a combination of ductile CuCrZr matrix with W particles, which increase tensile strength as well as provide large capacity for uniform elongation and work hardening. This material will be referred to as „W-particle“.
- CuCrZr alloy doped with vanadium (0.221%) is characterized by different precipitations compared to CuCrZr and therefore leads to the enhancement of high temperature creep strength. Given the vanadium doping, this material will be referred to as „V-doped“.
- ODS-Cu in this case is pure copper strengthened with Y2O3 ODS particles industrially produced using parameters for alumina reinforced ODS materials. This material will be referred to as „ODS“.

The basic physical properties, such as density, thermal conductivity and fraction of CuCrZr (relevant for the studied composition) are summarized in Fig. 1. The information on ITER specification CuCrZr in various heat treatment states is also included.

### 2.3. Irradiation

Neutron irradiation was performed in the BR2 Belgian Material Test Reactor inside a fuel element in the radial position close to the reactor center and in the mid-plane horizontal position where the fast neutron ( $E > 0.1$  MeV) flux is  $4 \times 10^{14}$  n/cm<sup>2</sup>/s at a power of 60 MW. The samples were encapsulated in 1.5 mm steel tube filled with He. The gap between the samples and the tube was adjusted to achieve the target temperature following the thermal and neutronic calculations. The irradiation dose was calculated by MCNPX 2.7.0 [24] and found to be 2.15 dpa, 2.5 dpa, and 2.55 dpa (1.02–1.25 dpa in W) for the capsules with the samples irradiated, at 150 °C, 350 °C and 450 °C, respectively, also summarized in Table 2. For the materials containing W, the transmutation of Re and Os is calculated based on the ALEPH code developed by SCK CEN and available nuclear databases [25–29]. The concentration of Re in W after irradiation is 2.0–2.2 at.% and Os concentration is about 0.2 at.% (depending on the specific capsule).

The tensile samples have a flat-type dog bone geometry with a total length of 16 mm and the dimensions of the grip section is a width of 4.2 mm and a thickness of 1 mm. The gage length is 5.2 mm and the gage cross-section is  $1 \times 1.5$  mm<sup>2</sup>. Given the fine microstructure of the materials (grain size is less than 100  $\mu\text{m}$ ), the applied gage section area is sufficient to be representative of the material tensile properties (i.e. certainly more than ten grains per cross-section area). The description of irradiation capsules and sample payload is provided in Annex 1.

### 2.4. Mechanical and microstructural testing

The uniaxial tensile tests of the irradiated and non-irradiated small dog-bone-shaped specimens were carried out in air using Instron universal test machines equipped with furnace. The test temperature for the irradiated specimens ranged from RT to 450 °C. The overall length of the specimens was 16 mm with a gage length  $G$  of 5.2 mm. The initial cross section  $A_0$  of the samples was 1.60 mm<sup>2</sup> ( $W = 1.6$  mm  $\times$   $T = 1.0$  mm) for the un-irradiated and irradiated samples. The exact initial cross section for each sample was measured by profile projector.

The constant displacement speed of the pull rod was 0.2 mm/min, which corresponds to a strain rate of  $6 \times 10^{-4}$  s<sup>-1</sup>. The load  $F$  versus gage length elongation  $D_{tensile}$  was continuously measured during the test. The engineering strain was calculated as:

$$\epsilon_{eng} = \frac{D_{tensile}}{G} \quad (1)$$

The engineering stress was derived following the equation:

$$\sigma_{eng} = \frac{F}{A_0} \quad (2)$$

Fracture strain was evaluated as [30]:

$$\epsilon_{pl} = \ln\left(\frac{A_0}{A}\right) \quad (3)$$

where  $A_0$  and  $A$  are the minimum cross-section areas of the gage before testing and after fracture.

Fracture stress was evaluated as the load at fracture divided by the cross-section area  $A$  at fracture. The latter was measured by SEM applied on the fractured samples. More information is provided in Annex 1.

It is known that high temperature tests on Cu-based alloys may involve certain oxidation effects, which might affect the interpretation of the test result. A study of the oxidation of the surface of copper exposed to annealing at 200 and 300 °C up to few hours was performed [32]. The results showed that oxygen penetrates up to 1  $\mu\text{m}$  at 200 °C for 6 h, and up to 3  $\mu\text{m}$  at 300 °C. Furthermore, the oxidation of Cu sheets was studied in the temperature range of 200–1000 °C [32]. The study has revealed that the oxidation at temperatures below 200 °C leads to the formation of a thin layer of copper oxide, mainly of cuprous oxide (Cu<sub>2</sub>O). Oxidation at 300 °C promoted growth of a passivating oxide layer composed of CuO and Cu<sub>2</sub>O. In the temperature range from 400 to 700 °C, the passivating copper oxide layer was fragile and showed poor adherence to the Cu surface. The oxidation at higher temperatures promoted complete oxidation of the Cu sheets. Given that the present tests are performed up to 450 °C and the thickness of the sample is 1 mm, the oxide layer is likely formed on the surface of tensile samples. However, its impact on the bulk mechanical properties is deemed to be minor.

## 3. Results

In the following, first, the mechanical properties of the materials in non-irradiated state will be presented, compared and discussed. Then, the effect of the neutron irradiation on the change of the mechanical properties will be shown. Finally, the analyses of the fracture surfaces and the effect of the irradiation on it will be presented. For the two non-composite materials, i.e. V-doped and ODS Cu, a detailed analysis of the fracture surface with the derivation of the cross-section area after the fracture and calculation of the true stress at fracture has also been performed, which can be helpful for the reconstruction of true stress – strain properties of the materials. This characterization would be meaningless for the composite materials (given that each material constituting the composite has its individual mechanical performance) and therefore it was not applied for the composites studied here.



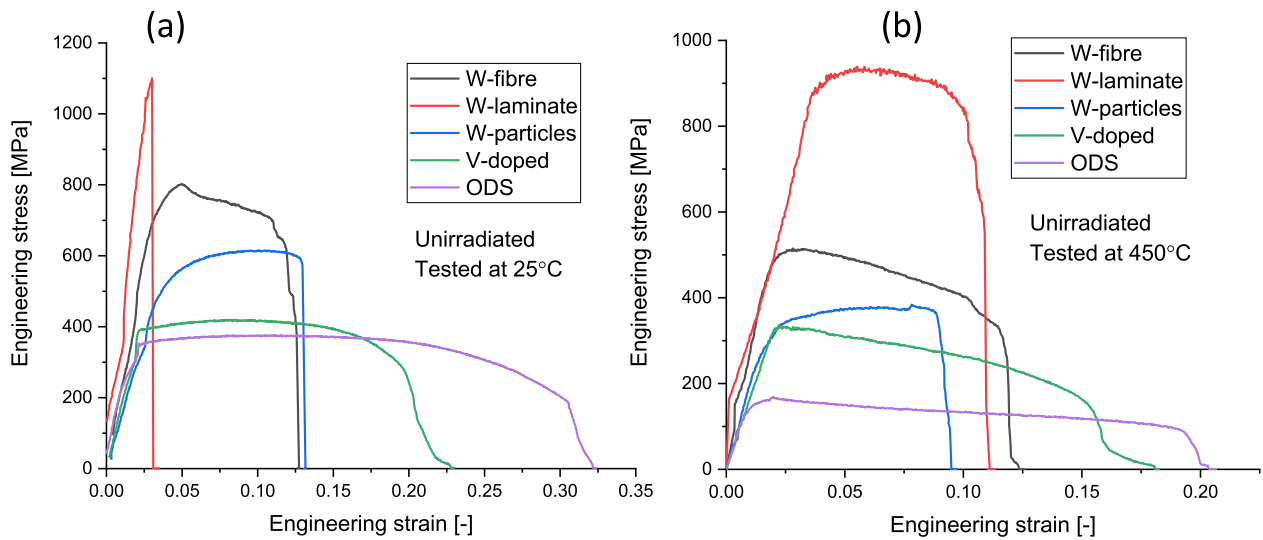


Fig. 2. Stress-strain data on non-irradiated materials obtained at (a) 25 °C and (b) 450 °C.

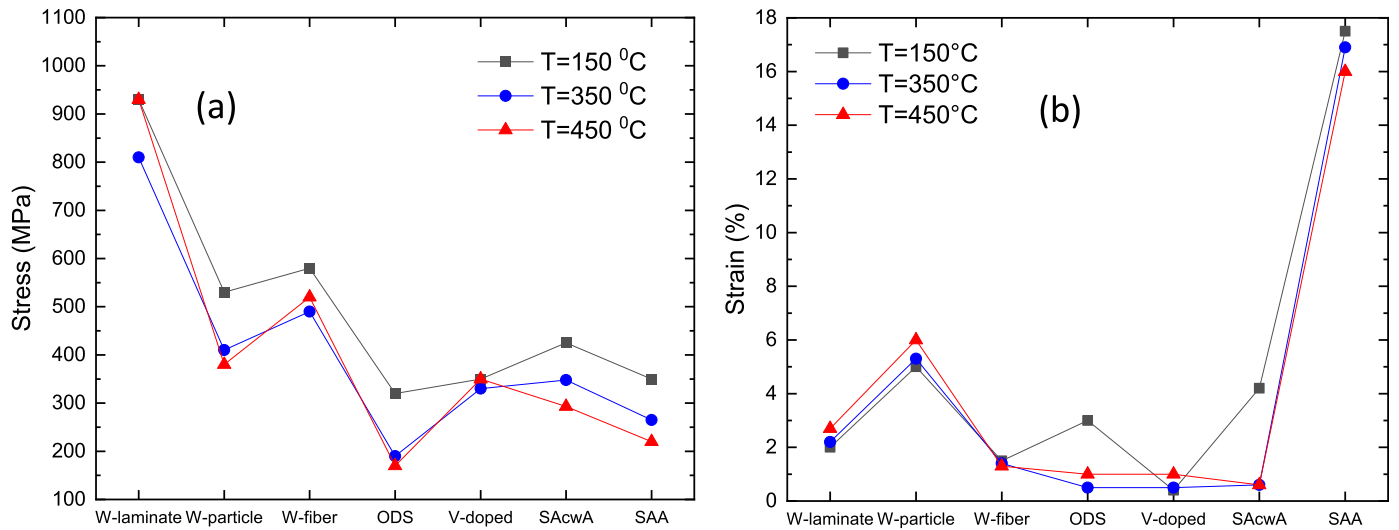


Fig. 3. (a) UTS in the temperature range of 150–450 °C for the advanced Cu-based alloys and reference ITER-specification CuCrZr in two post-heat treatment conditions. For the SACwA and SAA heat treatment conditions of CuCrZr the average UTS is presented as reviewed in [7]. (b) Uniform elongation in the temperature range of 150–450 °C for the advanced Cu-based alloys and reference ITER-specification CuCrZr in the SACwA and SAA annealing condition (the data for SACwA and SAA is taken from [16]).

### 3.1. Mechanical properties in the non-irradiated state

The reference (i.e. non-irradiated state) stress-strain curves are shown in Fig. 2a-b-c-d for 150 and 450 °C test temperatures, the figures for other studied test temperatures are provided in Annex 2. The obtained results were found to be quite reproducible from one sample to another (spread of the curves within 5%) and therefore only one curve per material is shown in each sub-figure. From the presented data on the non-irradiated materials several conclusions can be drawn.

First of all, the W-laminate has the highest strength among all the tested materials. However, the material is brittle at room temperature, but it becomes ductile at 150 °C. It should be noted that the brittleness at RT is not linked to the intrinsic properties of the W foil, as the latter is ductile at RT [33], but rather defined by the microstructure of the foil after the thermo-mechanical treatment applied to fabricate the composite. Clearly, the mechanical response of this composite is governed by the mechanical properties of the tungsten foils.

The W-fiber material renders a considerable strength, being the second strongest material after the W-laminate. Due to the specific

strengthening mechanism, the material exhibits essentially limited uniform elongation (compared to the baseline CuCrZr), which is dictated by the properties of the strengthening element i.e. W wire. Indeed, it is known that W wire applied in this composite has rather low uniform elongation (as revealed by the individual tests of the fibers under tension) [34]. The strength of W-fiber material progressively decreases with rising the test temperature without a recovery of the uniform elongation, which is in line with the evolution of the tensile properties of the W wire [34].

Contrary to the two above discussed materials, the W-particle grade appears to have a lower strength but a high work hardening capacity. This means that the plastic deformation is controlled by dislocation slip in the CuCrZr matrix, while W particles act as strengthening non-coherent precipitates (W has bcc structure, while Cu has fcc structure). Size/density particle distribution likely controls the UTS. Since the post-necking deformation of this material is very limited, one can assume that the void nucleation and coalescence of voids near the W particles promote the formation and propagation of the microcracks. Should the size/density of W particles change (e.g. due to the

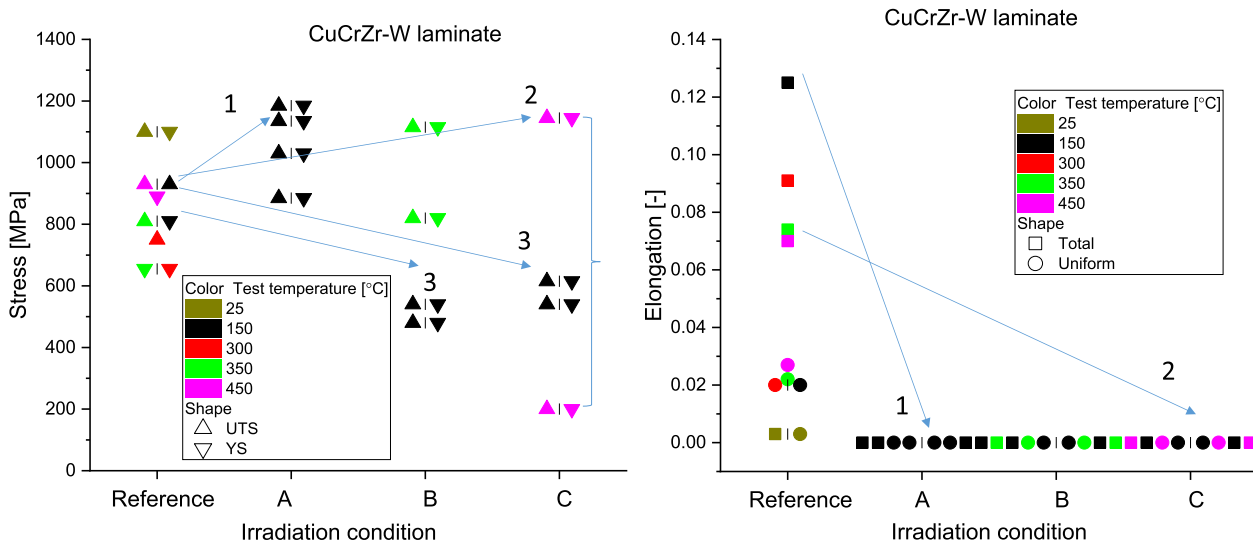


**Fig. 4.** Effect of the irradiation on the UTS/YS and total/uniform elongation of W-laminate material. The details of the irradiation conditions are provided in Table 2. The arrows are added to guide an eye reflecting the most prominent effects, namely: (1) Significant low temperature hardening at  $T_{irr}=150\text{ }^{\circ}\text{C}$  and complete loss of total elongation. (2) Significant scatter of strength after the irradiation at  $450\text{ }^{\circ}\text{C}$ , complete loss of total elongation. (3) At  $T_{test}=150\text{ }^{\circ}\text{C}$ , the irradiation at  $350\text{ }^{\circ}\text{C}$  and  $450\text{ }^{\circ}\text{C}$  causes loss of fracture strength.

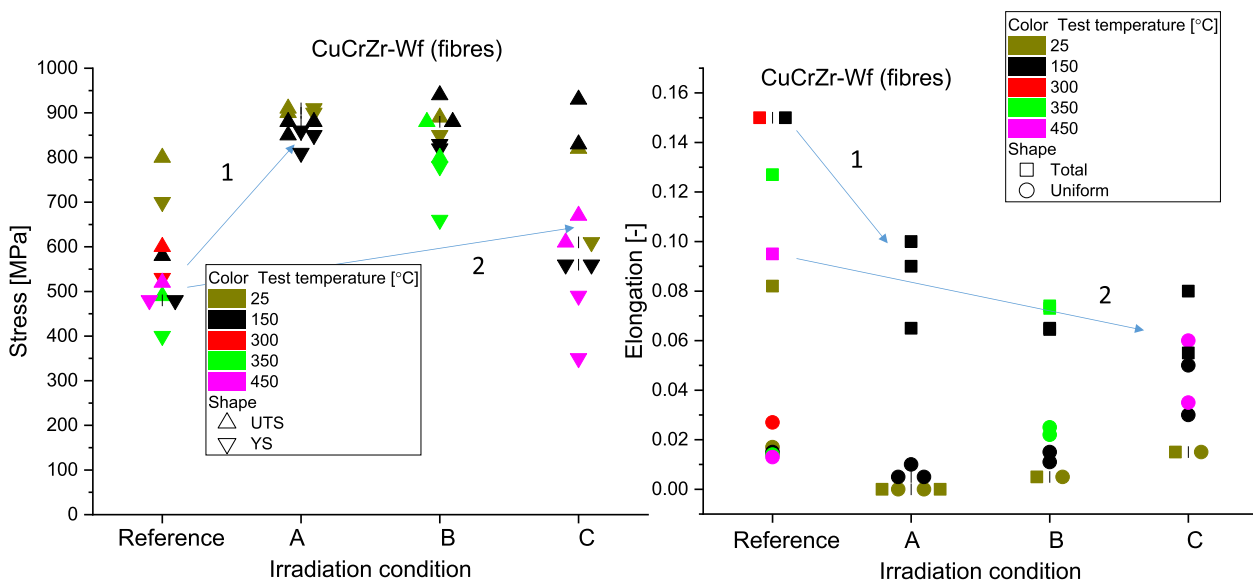


**Fig. 5.** Effect of the irradiation on the UTS/YS and total/uniform elongation of W-fiber material. The details of the irradiation conditions are provided in Table 2. The arrows are added to guide an eye reflecting the most prominent effects, namely: (1) Strong low temperature hardening at  $T_{irr}=150\text{ }^{\circ}\text{C}$  and loss of total elongation implying embrittlement of the fibers. (2) At  $T_{irr}=450\text{ }^{\circ}\text{C}$ , the strength is preserved after the irradiation, with a presence of ductile fiber deformation.

irradiation), the UTS and post-necking deformation would be affected as well.

The V-doped CuCrZr has a negligible uniform elongation at  $150\text{ }^{\circ}\text{C}$  and above. At RT, the uniform elongation is about 10%. One peculiar feature of this material is that the yield stress (and UTS) is almost constant in the temperature range  $150\text{--}450\text{ }^{\circ}\text{C}$ . Such feature may point to the reorganization of Cr-Zr-V precipitates depending on the temperature, such that an increase of the test temperature does not lead to a reduction of the yield stress.

Finally, the  $\text{Y}_2\text{O}_3\text{--ODS}$  material has the lowest strength but the highest total elongation among the tested grades. Unlike the V-doped grade, the ODS material exhibits pronounced reduction of the yield stress with an increase of the test temperature.

To enable a comparison of the mechanical properties of the advanced grades with the conventional ITER specification CuCrZr, the UTS and

uniform elongation values are summarized in Fig. 3(a) and Fig. 3(b). In terms of the strength, all advanced grades, except the ODS material, outperform the baseline CuCrZr. The UTS of V-doped grade is comparable to the SACwA condition.

The uniform elongation is provided in Fig. 3(b). The uniform elongation of the SAA CuCrZr ranges between 15 and 18% in the temperature range  $\text{RT--}450\text{ }^{\circ}\text{C}$  [35], which means that all advanced grades have considerably smaller values. In the case of SACwA heat treatment, the uniform elongation is 4% at  $150\text{ }^{\circ}\text{C}$  and it decreases down to zero at  $300\text{ }^{\circ}\text{C}$  [36]. In terms of the uniform elongation, on Fig. 3(b) we can see W-laminate and W-particle grades exhibit a larger uniform elongation as compared to ITER specification CuCrZr, especially at the high temperature side, which clearly reflects the improvement of the high-temperature performance.

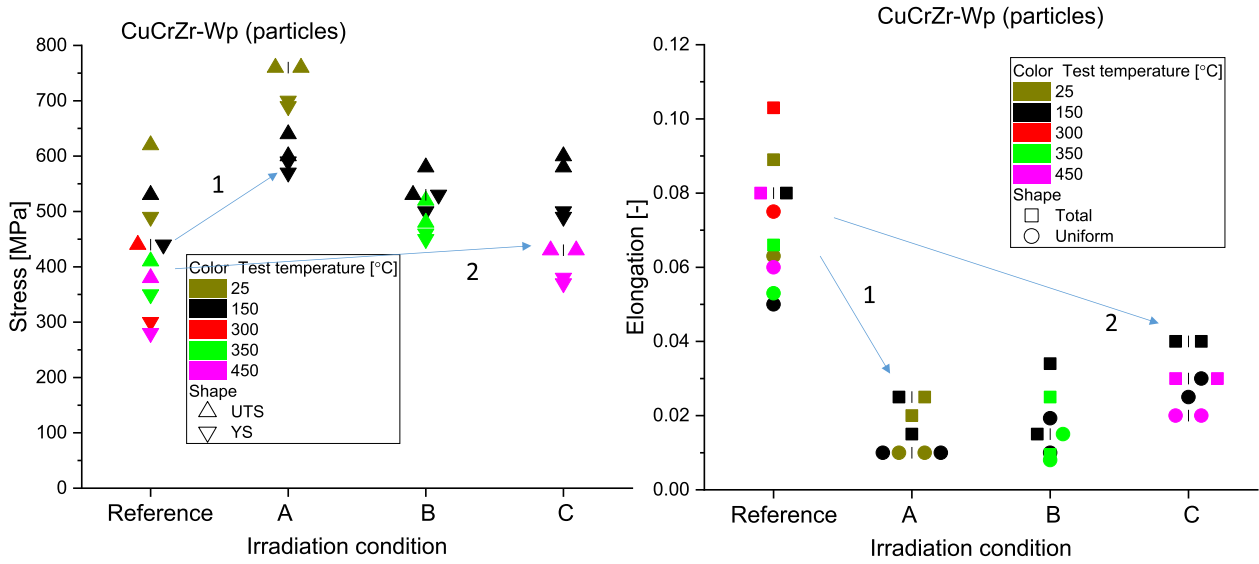


**Fig. 6.** Effect of the irradiation on the UTS/YS and total/uniform elongation of W-particle material. The details of the irradiation conditions are provided in Table 2. The arrows are added to guide an eye reflecting the most prominent effects, namely: (1) Low temperature hardening at 150 °C and loss of uniform elongation. (2) At  $T_{irr}=450$  °C, the strength is preserved after irradiation, but with loss of uniform elongation.

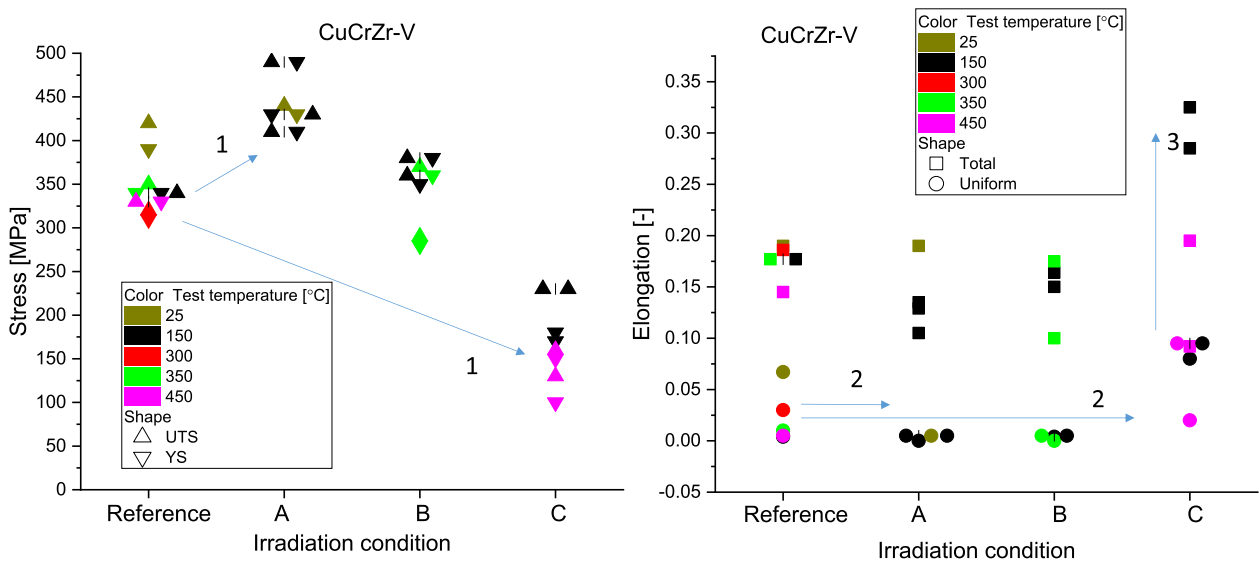


**Fig. 7.** Effect of the irradiation on the UTS/YS and total/uniform elongation of V-doped material. The details of the irradiation conditions are provided in Table 2. The arrows are added to guide an eye reflecting the most prominent effects, namely: (1) Low temperature hardening at 150 °C and high temperature softening at 450 °C. (2) No strong effect on the initially low uniform elongation at 150–450 °C. (3) Recovery of total elongation at  $T_{test}=150$  °C after irradiation at 450 °C.

### 3.2. Mechanical properties in the irradiated state

The mechanical tests after the irradiation were performed at two temperatures, namely at the irradiation temperature and 150 °C, whilst the latter is considered as the lower boundary temperature for the operation in DEMO divertor cooling pipes. We shall first present the results for  $T_{irr} = T_{test}$  and then  $T_{test} = 150$  °C. Given that at  $T_{irr} = 150$  °C some spare samples were available, extra tests were also performed at RT. The effects of the irradiation and test temperature on the tensile strength, uniform and total elongation are all together visualized in Fig. 4 (W-laminate), Fig. 5 (W-fiber), Fig. 6 (W-particle), Fig. 7 (V-doped), Fig. 8 (ODS) for each material separately. The figure captions also collect the most important messages regarding the discovered irradiation effects. For the sake of brevity, the engineering stress-strain curves are collected in Annex 2, while observations made based on those results are summarized below.

At  $T_{irr} = T_{test} = 150$  °C, we can reveal embrittlement of the W-laminate material, which fractures without any plastic deformation. The W-fiber material exhibits an increase of the yield stress (i.e. irradiation hardening) and the rise of UTS is by a factor of two with only a moderate reduction of the total elongation. W-particle material exhibits irradiation hardening, which is, however, more moderate ( $\Delta\sigma_{UTS}$  is 100 MPa) as compared to the two other composites. Also, the uniform elongation of W-particle material drops down from 5% to 1%. The irradiation hardening in V-doped material is the same as in W-particle ( $\Delta\sigma_{UTS}$  is 100 MPa) with almost no change in the uniform elongation, which was only 0.5% before irradiation. The incurred irradiation hardening did not essentially alter the extensive post necking deformation, which also occurred in the non-irradiated state. The ODS material exhibits considerable irradiation hardening (UTS increases by 70%) and uniform elongation reduces down to 0.5%, although the post-necking deformation yields ~8% of the total elongation. In fact, the mechanical

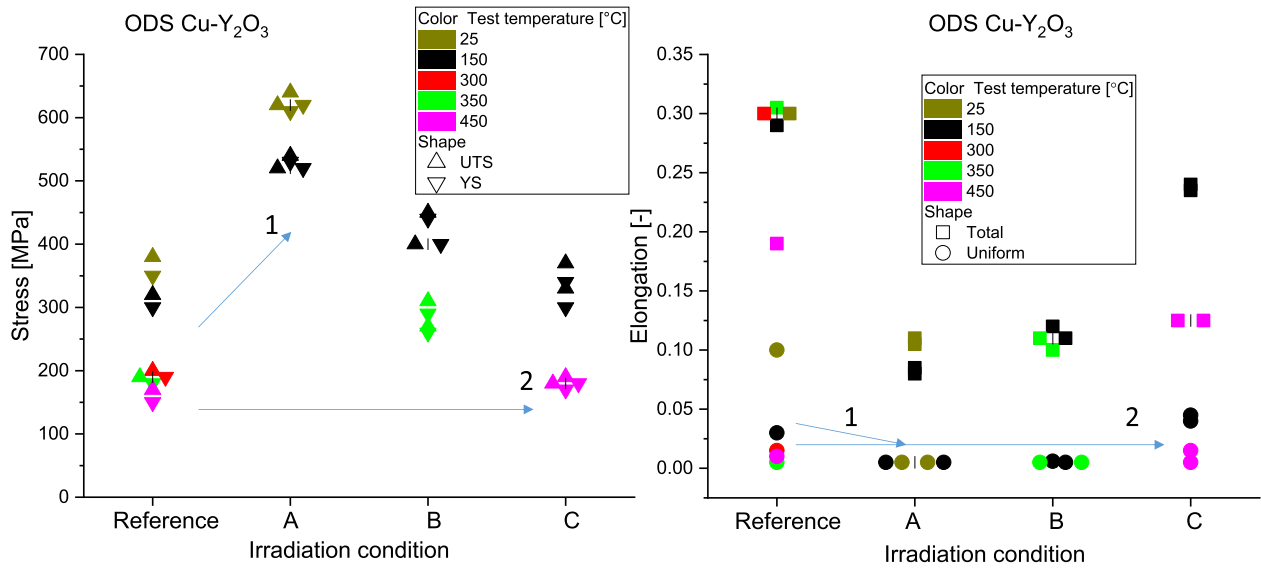


**Fig. 8.** Effect of the irradiation on the UTS/YS and total/uniform elongation of ODS material. The details of the irradiation conditions are provided in Table 2. The arrows are added to guide an eye reflecting the most prominent effects, namely: (1) Low temperature hardening at 150 °C and complete loss of uniform elongation. (2) At  $T_{\text{irr}}=450$  °C, the strength (and low uniform elongation) is preserved.

performance of V-doped and ODS grades becomes comparable after irradiation at 150 °C.

Test results at  $T_{\text{irr}} = T_{\text{test}} = 350$  °C show that the W-laminate material remains fully brittle and the stress at fracture, being 800 and 1100 MPa (for the two samples tested) is comparable to the one measured at  $T_{\text{irr}} = T_{\text{test}} = 150$  °C. The response to the tensile load of the W-fiber material is also similar at 350 and 150 °C, meaning a comparable increase of the UTS and insignificant reduction of the total elongation. An interesting observation is that the uniform elongation has slightly increased after the irradiation at 350 °C. This could be explained by the irradiation hardening of the W fibers, which enables to reach a slightly higher strain in the composite prior to the UTS point. In the case of W-particle material, the UTS at  $T_{\text{irr}} = T_{\text{test}} = 350$  °C is lower than at 150 °C, and the uniform elongation is reduced down to 1.5% (from 6% in the non-irradiated state). The fracture occurs shortly after the UTS, which is also the case for  $T_{\text{irr}} = T_{\text{test}} = 150$  °C and the tests in the non-irradiated state. V-doped material exhibits slight irradiation softening ( $\Delta\sigma_{\text{UTS}}$  is

25 MPa), and negligible uniform elongation (0.5%). In the case of ODS material, the hardening is 100 MPa, which by a factor 2 lower compared to the results at  $T_{\text{irr}} = T_{\text{test}} = 150$  °C. However, the uniform elongation still remains very small, i.e. only 0.5%. Overall, for most of the properties of the studied materials, the effect of the irradiation at 150 and 350 °C is rather similar, except for (i) enhancement of the uniform elongation of the W-fiber material up to 2.5% (exceeding the one before the irradiation) at  $T_{\text{irr}} = T_{\text{test}} = 350$  °C and (ii) essential reduction of the irradiation hardening in ODS material at  $T_{\text{irr}} = T_{\text{test}} = 350$  °C compared to the results at 150 °C.

The increase of the irradiation temperature up to 450 °C, makes more prominent effect on the mechanical properties. The W-laminate composite still demonstrates fully brittle behavior. W-fiber material appears to exhibit a significant reduction of the UTS (compared to results at  $T_{\text{irr}} = T_{\text{test}} = 350$  °C) and an increase of the uniform elongation up to 5%. During the post-necking deformation, the composite was so strong that instead of the rupture of the wires in the neck, a shoulder of a grip end of the specimen was sheared off. It was therefore not possible to determine the total elongation or area reduction for the W-fibers in this test condition. In the case of the W-particle material, the effect of the increase of the irradiation temperature is minor, and it is mainly expressed in the recovery of the uniform elongation and reduction of the UTS. In the V-doped material, the irradiation at 450 °C leads to a pronounced (more than a factor of two) reduction of the UTS from 336 MPa (in non-

irradiated state) down to 145 MPa. As a result of this softening, the uniform elongation reaches 5%, while it amounts only to 1% before the irradiation. Modification of the structure and/or size/density distribution of strengthening particles could be an explanation for such a strong softening effect. The ODS material retains the UTS and uniform elongation to be very close to the non-irradiated values.

In addition to  $T_{\text{irr}} = T_{\text{test}}$  condition, a set of data has been obtained at  $T_{\text{test}} = 150$  °C, while the irradiation temperature was 350 °C (see Fig. 23) and 450 °C (see Fig. 24). The following findings were noticed as outcomes of the results presented on these two figures. The fracture stress (in this case, the same as UTS) of W-laminates reduces down to ~500–600 MPa, i.e. even lower than the UTS of the non-irradiated material. This implies that the suppression of the micro-yielding due to the irradiation defects differs at 150 °C and higher test temperatures. As a result, the W-laminate material irradiated at high temperature exhibits a loss of strength at 150 °C, and the fracture is purely brittle irrespective of the irradiation and test temperature. Secondly, we can see that the softening of the V-doped material irradiated at 450 °C remains for the tensile test at 150 °C. This implies that the softening truly comes from the change of the material microstructure and not just from the dislocation-defect interaction, where the softening could be explained by assistance of thermal activation to overcome specific irradiation defects or irradiation modified Cr-Zr-V precipitates. The mechanical performance of W-fiber, W-particle and ODS materials remains similar at  $T_{\text{test}} = T_{\text{irr}}$  and 150 °C.

Finally, a set of tests was done at  $T_{\text{test}} = \text{RT}$  and  $T_{\text{irr}} = 150$  °C, as presented in Fig. 25. For the W-fiber material, the reduction of the test temperature to RT has resulted in the brittle fracture. This is quite an important result, because at  $T_{\text{irr}} = T_{\text{test}} = 150$  °C the composite remains ductile with a considerable uniform and total elongation. Hence, the ductile to brittle transition for the W fibers irradiated at 150 °C up to ~2.5 dpa is in the range RT–150 °C. The W-particle material experiences significant irradiation hardening and the reduction of the uniform elongation by about factor of three. V-doped and ODS materials exhibit irradiation hardening with immediate necking after the yield (i.e. zero uniform elongation), but preserve extended post-necking deformation. The irradiation hardening in the ODS material is about 70%, while in the V-doped material it is only 5%. The W-laminate material has not been tested at RT given that it was found to be brittle even at higher temperature.



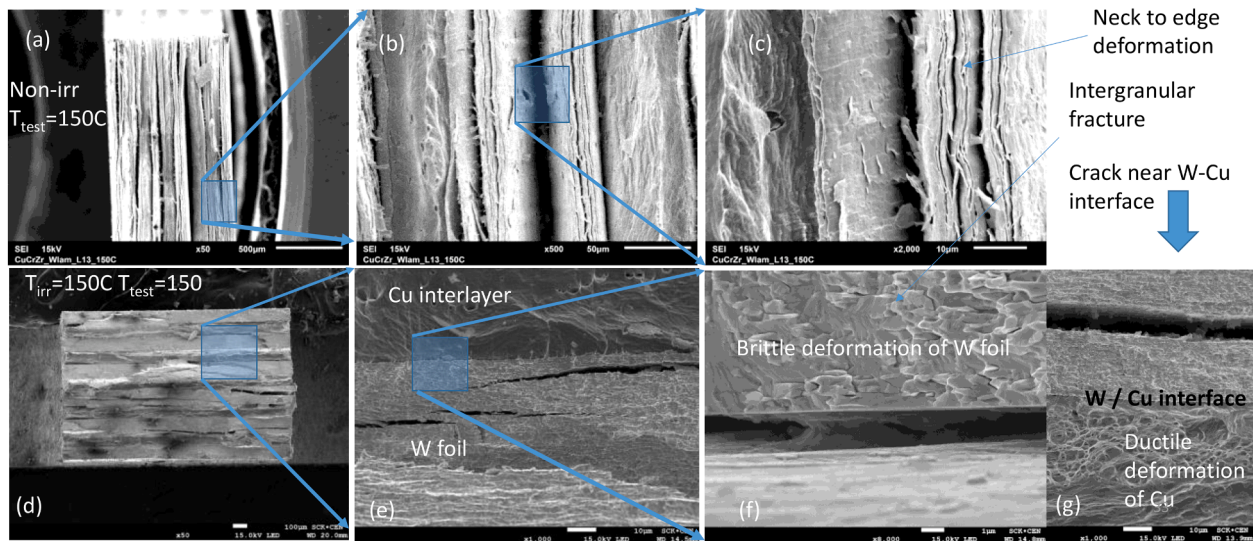


**Fig. 9.** SEM micrographs showing the typical fracture surface of W-CuCrZr laminates in the reference (upper pane) and irradiated (lower pane) states tested at 150 °C. The upper pane shows a series of zoomed images extracted in tungsten region from macro-view (500  $\mu\text{m}$  scale bar, a) to meso-scale view (50  $\mu\text{m}$  scale bar, b) and down to micro-scale (10  $\mu\text{m}$  scale bar, c), the latter shows a pattern of the neck-to-edge tungsten grains. A zoomed area is shown as blue-filled rectangular. The lower pane shows a series of zoomed images extracted in W-Cu interface from macro-view (100  $\mu\text{m}$  scale bar, d) to meso-scale view (10  $\mu\text{m}$  scale bar, e) and down to micro-scale (1  $\mu\text{m}$  scale bar, f). Fig.(g, magnification scale is 10  $\mu\text{m}$ ) shows the ductile dimples on the Cu part near the W-Cu interface and the presence of microcrack in W part.

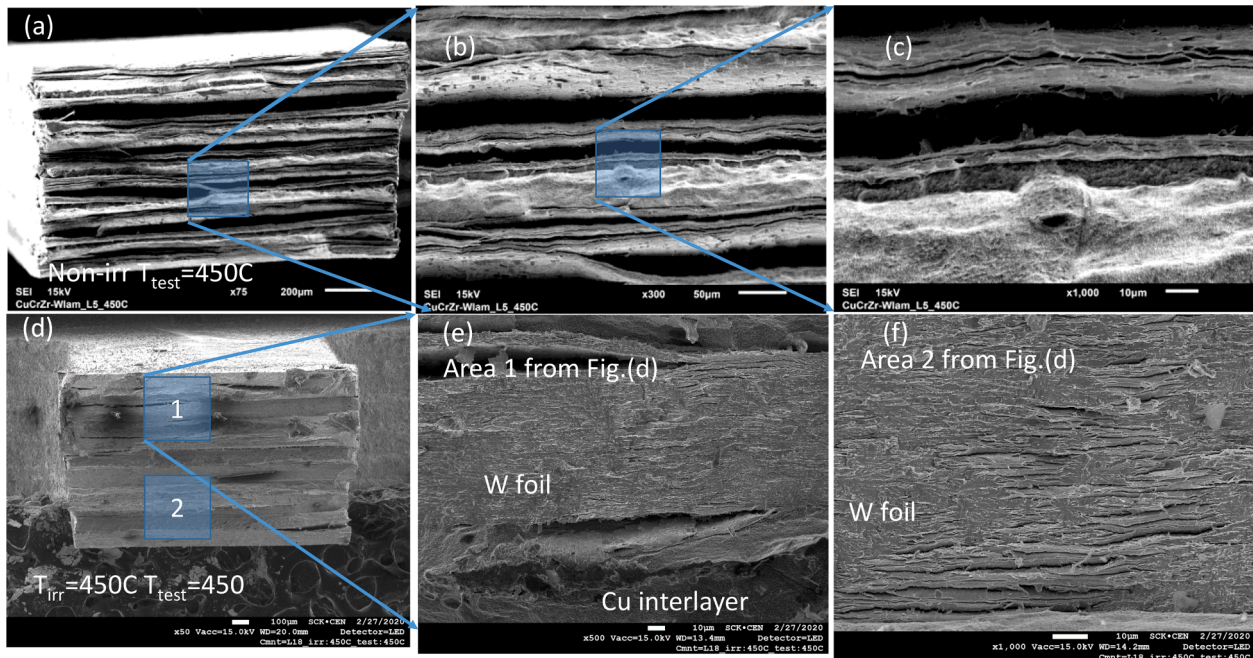


**Fig. 10.** SEM micrographs showing the typical fracture surface of W-CuCrZr laminates in the reference (upper pane) and irradiated (lower pane) states tested at 450 °C. Fig.(a) is a macro-view (200  $\mu\text{m}$  scale bar), Fig.(b) has 50  $\mu\text{m}$  scale bar, Fig.(c) has 10  $\mu\text{m}$  scale bar, Fig.(d) has 100  $\mu\text{m}$  scale bar, Fig.(e) and (f) has 10  $\mu\text{m}$  scale bar.

### 3.3. Fracture surface analysis

The fracture surface of the W-laminate material in the reference and 150 °C-irradiated condition tested at 150 °C is shown in Fig. 9. The fracture of the reference sample occurs by the delamination and necking of individual tungsten grains, which is fully consistent with the original work [18] where the authors have developed this composite. The CuCrZr interlayers exhibit fracture by dimple rupture, which is a normal fracture mode for this material. After the irradiation, CuCrZr-interlayers still show ductile deformation with well-resolved dimples, while W foils

exhibit brittle intergranular fracture with large lateral cracks emerging near the W-CuCrZr interfaces. Examples of such cracks are shown for two different fracture areas on Fig. 9(g). The cracks are extended along the W-Cu interface but there is no delamination between Cu and W. This means that the formation of cracks inside the W foil occurs prior the stress level exceeds the W-Cu interface bond strength. This indicates that the primary impact of the irradiation damage at 150 °C is expressed in the embrittlement of the W foil. Here, we need to note that the irradiation embrittlement of the laminate composite has been reported earlier by Garrison et al. [37]. In that work, the irradiation was performed at



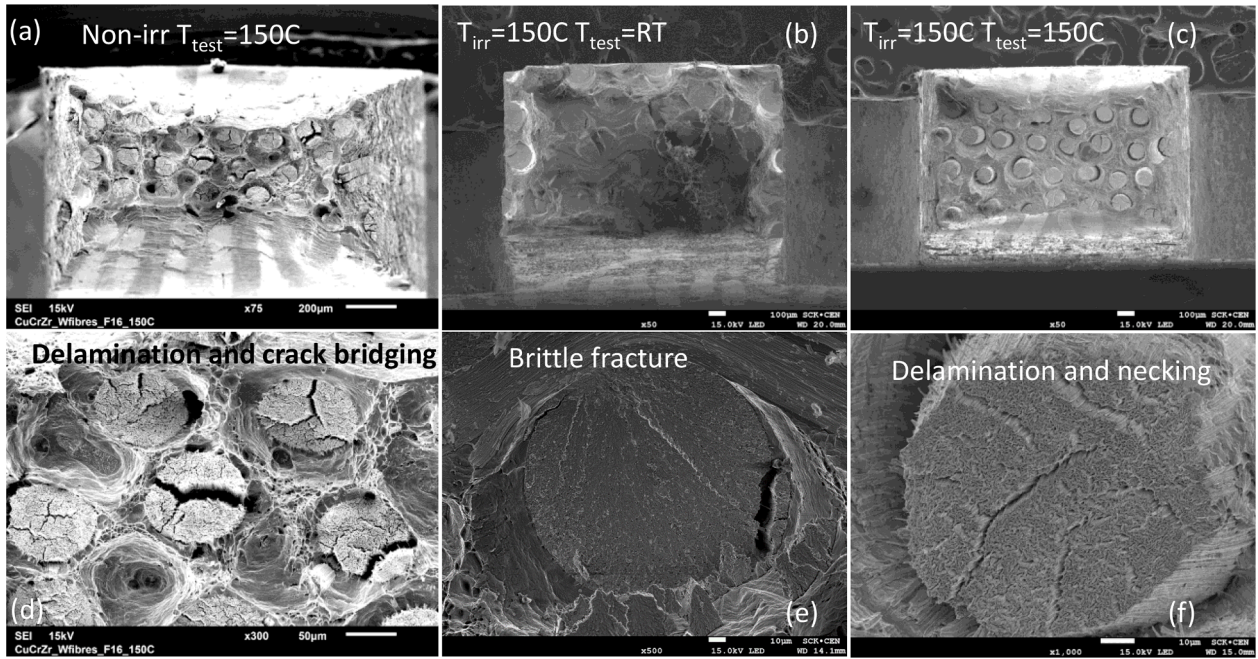


Fig. 11. SEM micrographs showing the typical fracture surface of W fiber-reinforced CuCrZr irradiated at 150 °C, test temperature is specified on the figure legends. Fig.(a) has 200  $\mu\text{m}$  scale bar, Fig.(b) has 100  $\mu\text{m}$  scale bar, Fig.(b) has 100  $\mu\text{m}$  scale bar, Fig.(d) has 50  $\mu\text{m}$  scale bar, Fig.(e) and (f) has 10  $\mu\text{m}$  scale bar.

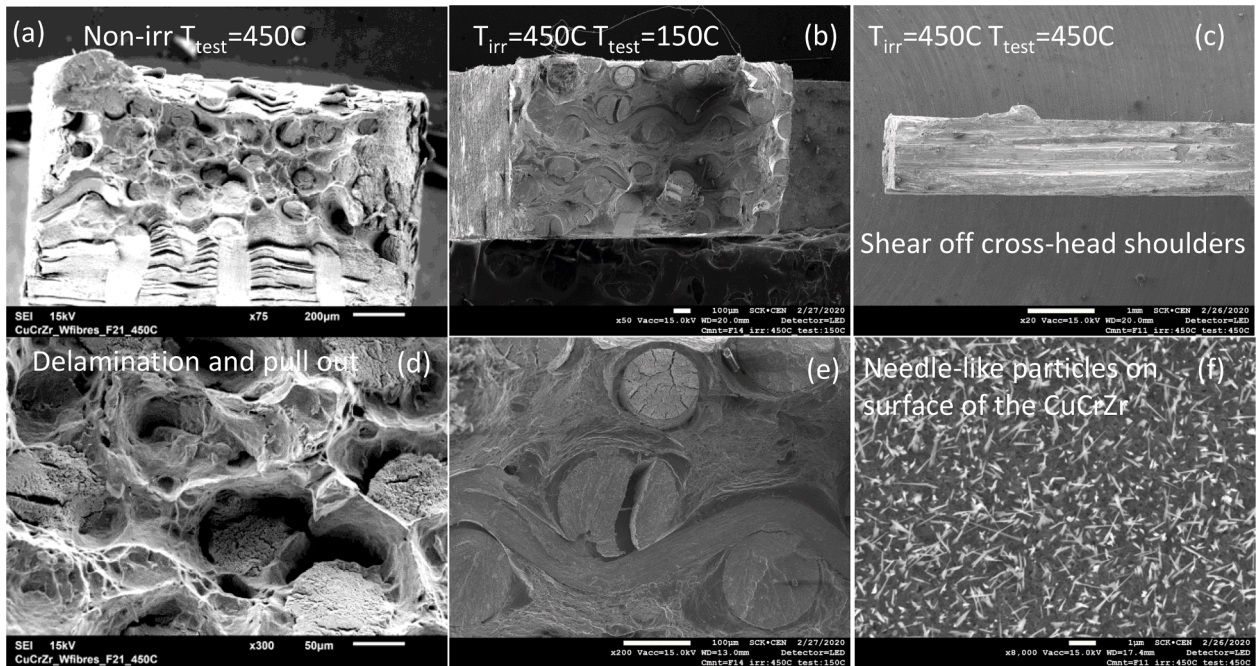


Fig. 12. SEM micrographs showing the typical fracture surface of W fiber-reinforced CuCrZr irradiated at 450 °C, test temperature is specified on the figure legends. Fig.(a) has 200  $\mu\text{m}$  scale bar, Fig.(b) has 100  $\mu\text{m}$  scale bar, Fig.(b) has 1000  $\mu\text{m}$  scale bar, Fig.(d) has 50  $\mu\text{m}$  scale bar, Fig.(e) has 100  $\mu\text{m}$  scale bar, Fig.(f) has 1  $\mu\text{m}$  scale bar.

higher ratio of thermal to fast neutrons, thereby causing a higher  $Re/Os$  generation rate in tungsten. The irradiation temperature was also higher (400–800 °C) than in this study. Yet, the present results demonstrate that a lower transmutation rate and irradiation temperature also leads to the severe irradiation embrittlement of this composite. A recent work performed by Zinovev et al. [38] reported the investigation of the bending tests of individual W foils irradiated up to 0.15 dpa (in W) at 400 °C, which showed no embrittlement of the foils. The foil were retained its ductility even at RT tests.

The features of the fracture surface of W-laminate tested at 350 °C are very similar to those at 150 °C shown in Fig. 9. The fracture surface of the W-laminate tested at 450 °C is shown in Fig. 10. The upper pane shows the microstructure in non-irradiated state, the lower in the as-irradiated state. The reference material fractures by delamination and the latter may occur either at the W-CuCrZr interface or within the W foil itself. Individual tungsten foils fracture by delamination and necking. A zoom-in of the delamination of W-CuCrZr interface is shown on the upper pane of Fig. 10. After the irradiation, no delamination of the W-



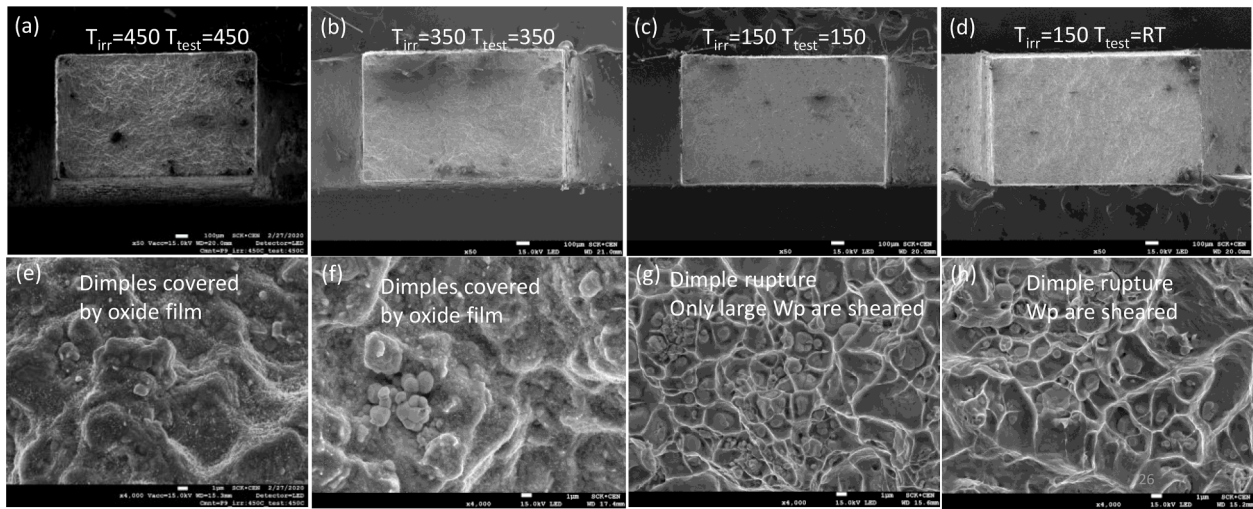


Fig. 13. SEM micrographs showing the typical fracture surface of W particle-reinforced CuCrZr irradiated and tested at different temperatures. The formation of oxide film is evident on (e) and (f). Figs.(a-d) have 100  $\mu\text{m}$  scale bar, Figs.(e-h) have 1  $\mu\text{m}$  scale bar.

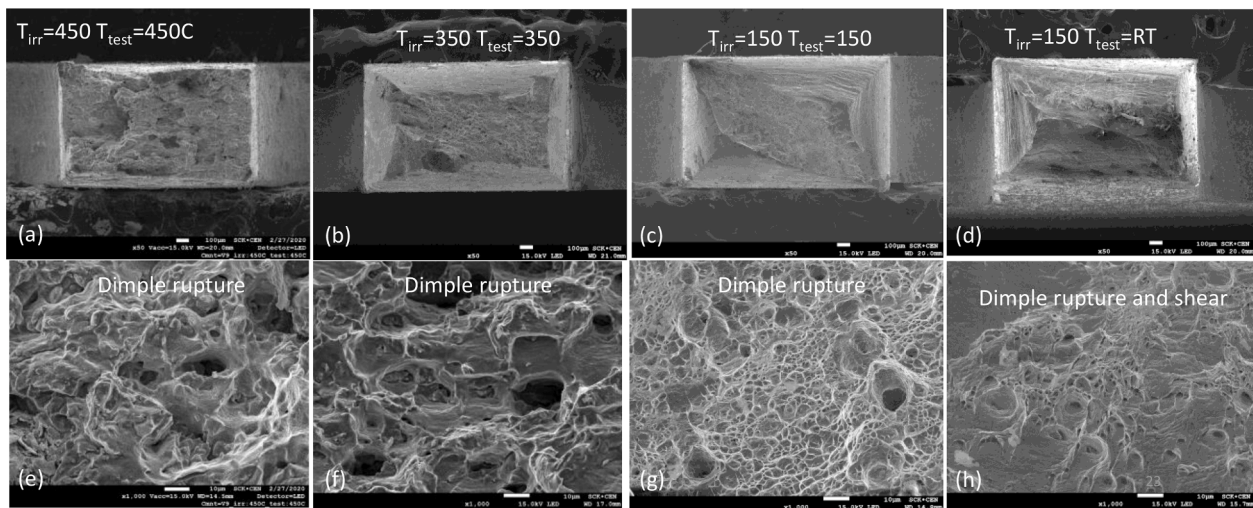


Fig. 14. SEM micrographs showing the typical fracture surface of V-doped CuCrZr irradiated and tested at different temperatures. Figs.(a-d) have 100  $\mu\text{m}$  scale bar, Figs.(e-h) have 10  $\mu\text{m}$  scale bar.

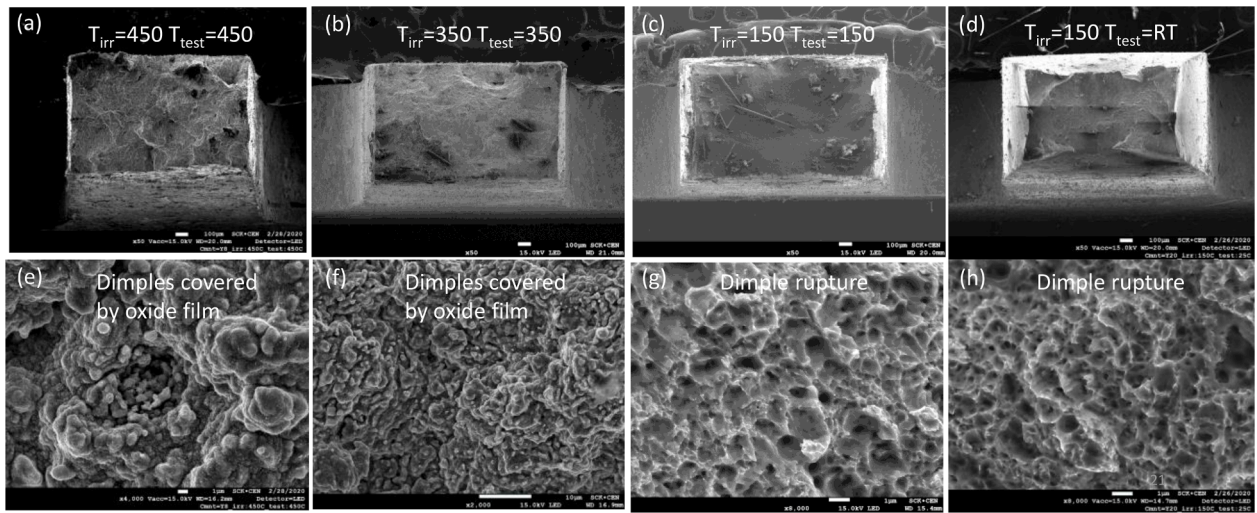
CuCrZr interface was observed. All inspected W-CuCrZr interfaces are free of cracks. CuCrZr interlayers exhibit ductile fracture. W foils exhibit mixed fracture surface, part of the foils are fractured by brittle cleavage, another part appears to have necking of the individual grains. Multiple small lateral cracks are present across the whole thickness of the foils, but large lateral cracks are found next to the W-CuCrZr interfaces, such as shown on the lower pane of Fig. 10.

Fig. 11 presents SEM micrographs of the typical fracture surface of W-fiber material irradiated at 150  $^{\circ}\text{C}$ , an example of the fracture surface in the non-irradiated state after testing at 150  $^{\circ}\text{C}$  is provided as well. In the non-irradiated state, macroscopic necking of the composite as well as individual necks on the tungsten fibers occurs. The fracture pattern registered in the non-irradiated fibers tested individually at RT and elevated temperature in Ref. [39] is very similar to what is found here. The surrounding copper matrix is deformed in a ductile mode by dimple rupture. The comparison of the fracture surface of the samples tested at RT and 150  $^{\circ}\text{C}$  after irradiation shows clearly that brittle fracture occurs in the W fibers at RT, while delamination and necking takes place at 150  $^{\circ}\text{C}$ . This observation confirms an earlier made suggestion that the ductile to brittle transition for the W fibers irradiated at 150  $^{\circ}\text{C}$  occurs between 150  $^{\circ}\text{C}$  and RT. The CuCrZr matrix remains ductile after

irradiation and the fracture mode is dimple rupture.

The fracture surface of the W-fiber samples tested after 450  $^{\circ}\text{C}$  irradiation is presented in Fig. 12. In the non-irradiated state, the fibers are pulled out and the fracture, as expected, occurs by necking and individual grain delamination. After irradiation, in the test at 150  $^{\circ}\text{C}$ , the macroscopic necking is considerably reduced and W fibers fracture either in a brittle way by cleavage or ductile manner by necking. A very similar fracture mode as shown in Fig. 21b and Fig. 21e is seen for  $T_{\text{irr}} T_{\text{test}} 350$   $^{\circ}\text{C}$ . At  $T_{\text{irr}} T_{\text{test}} 450$   $^{\circ}\text{C}$ , both tested samples did not rupture in the gage section, but instead the fibers were pulled out together with the cross-head. Accordingly, we could not investigate the fracture surface. Instead, we took the image of the CuCrZr matrix in the location of the pulled fiber (see Fig. 12(c)). In that location, we found numerous needle-like particles (see Fig. 12(f)) present only in the region of the contact of the fiber with the matrix. We did not observe such particles on any of the other CuCrZr matrices tested in this program. Due to a high residual activation of the samples, it was impossible to perform reliable chemical analysis by EDX to determine the chemical nature of those particles.

Fig. 13 presents SEM micrographs of the typical fracture surface of W-particle material irradiated and tested at different temperatures. The



**Fig. 15.** SEM micrographs showing the typical fracture surface of ODS ( $Y_2O_3$ -strengthened) Cu irradiated and tested at different temperatures. The irradiation temperature and test temperature are indicated on the figures directly for convenience. Upper pane shows a general view of the fracture sample. Lower pane shows high magnification of the fracture surface. The formation of oxide film is evident on (e) and (f). Figs.(a-d) have 100  $\mu m$  scale bar, Figs.(e,g,h) have 5  $\mu m$  scale bar, Fig. (f) has 10  $\mu m$  scale bar.

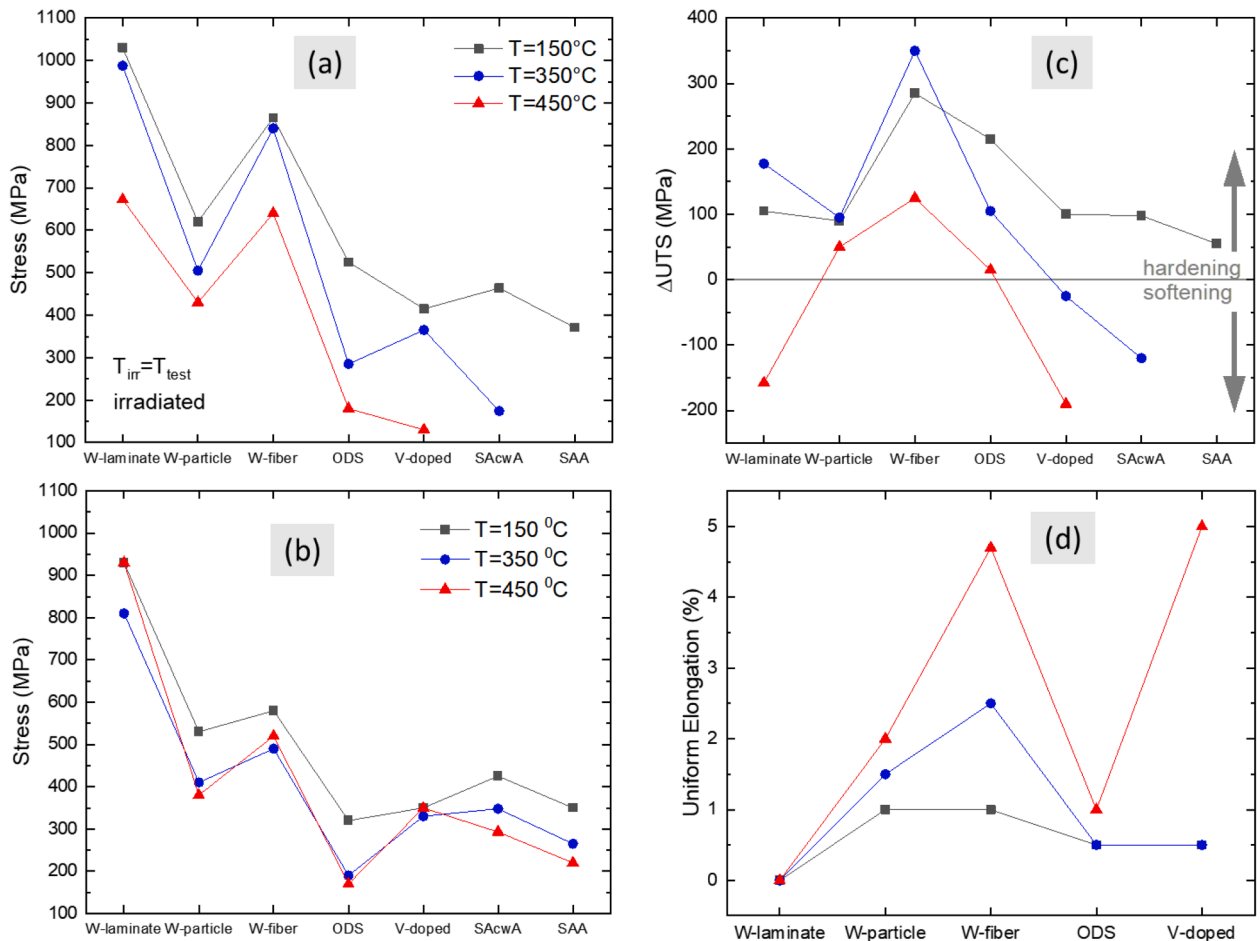


**Fig. 16.** Synthesis of the results indicating the effect of the irradiation on the studied materials. In the relevant figures, the irradiation temperature is equal to the test temperature. (a) UTS for the irradiated (upper pane) and (b) non-irradiated samples (lower pane). For the baseline ITER-specification CuCrZr in two heat treatments (SACwA and SAA) minimum tensile strengths are provided in the temperature range of 150–350  $^{\circ}C$  as collected in [7]. (c) change of the tensile strengths (upper pane) and (d) absolute value of the uniform elongation (lower pane).

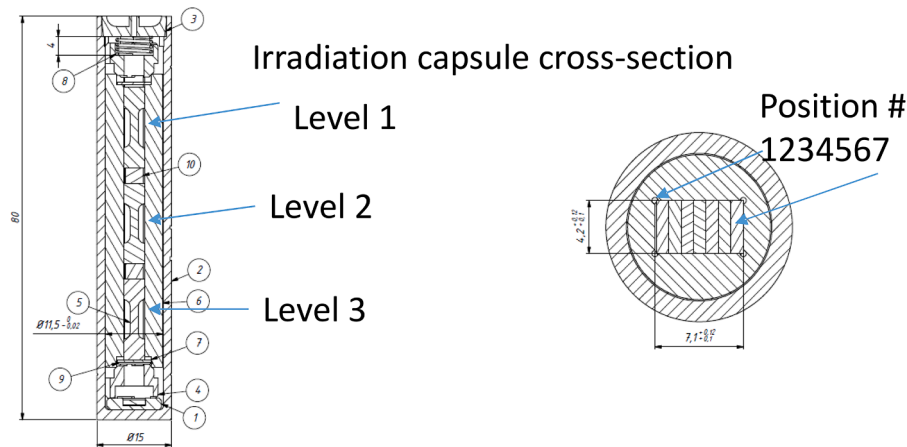


Fig. 17. Irradiation capsule vertical (level) and horizontal (position) cross-sections.

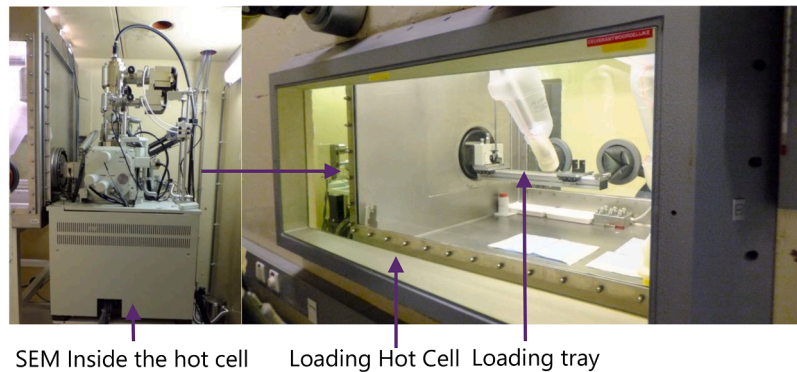


Fig. 18. The SEM inside a hot cell.

formation of the oxide film on the fracture surface is evident at 350 and 450 °C, see Fig. 13(e) and (f), respectively. This is natural oxidation of copper that should be expected at this temperature. No localized necking formation is seen at all applied irradiation and test conditions, which is consistent with very limited post-necking deformation of this material. At 150 °C and RT, the fracture surface consists of cells formed by the necked grains of the CuCrZr matrix and W particles. Based on the appearance (shape and fracture morphology) of the W particles on the fractured surface one can speculate on the mechanisms of the deformation occurred during the fracture. On Fig. 13(g), one can observe that large W particles have oval-like or elongated shapes, which suggests that these were sheared by multiple dislocation passage prior the fracture. The small particles keep their spherical shape, see Fig. 13(h). This can be interpreted as plastic deformation yielding to the accumulation of stress concentration near hard W particles, and the macroscopic crack opening is promoted once the micro-crack propagates through the W particles thereby cracking it and bridging micro-cracks. This fracture mechanism may explain why the post-necking deformation is limited in this material. We can also assume that small W particles remain un-sheared and they do not allow for the accumulation of significant stress concentration sufficient for the micro-crack formation next to the particles. According to the interpretation above, the propagating macro crack deflects around small W particles, which overall results in the formation of rather rough fracture surface. Judging from the visual inspection, the roughness increases with the test temperature, which can be interpreted that by increasing the test temperature the fracture of W particles is gradually suppressed (i.e. W particles may accommodate the exerted load by plastic deformation). The elongation also starts to recover with raising up the irradiation and test temperature. Yet, it is important to highlight that the above discussion on the deformation mechanisms

requires experimental confirmation by e.g. in-situ SEM experiments (although challenging to be performed on irradiated active samples).

Fig. 14 presents SEM micrographs of the fracture surface of V-doped grade. For this material, the oxidation was not pronounced as in the case of W-particle (compare with Fig. 13) and ODS materials (compare with Fig. 15). The dimple rupture and local shear were the two main fracture modes. Prior to the irradiation, the same fracture mode occurs, except that at  $T_{\text{test}} = 450 \text{ }^\circ\text{C}$  the sample exhibits neck to edge. After the irradiation, especially at  $T_{\text{irr}} = T_{\text{test}} = 150 \text{ }^\circ\text{C}$ , the area reduction is much smaller, which is consistent with the decrease of the total elongation. The dimension and density of dimples was increasing with increasing the irradiation-test temperature as well as the area reduction.

Fig. 15 collects the images of the fracture surface of the ODS material irradiated and tested at different temperatures. Irrespective of the irradiation and test temperature, the deformation is ductile since fracture surface is rough and full of dimples, clearly visible after tests at 150 °C and RT (see Fig. 15g and h). The oxidation of the fracture surface is very intensive already at 350 °C, which obscures the observation of the dimples' morphology. The intensive oxidation of this material is explained by the fact that pure copper is used for the matrix, while in other materials CuCrZr is applied, which enables the formation of a passivation layer (limiting the growth of Cu oxides). It is interesting to note that at RT, a localized necking deformation is observed (see Fig. 15d) resulting in the highest area reduction among all performed test conditions. At elevated temperatures, the post-UTS deformation mostly leads to the diffuse neck formation.

#### 3.4. Fracture stress and strain (for V-doped and ODS grades)

The extracted values of the true strain after fracture and true fracture



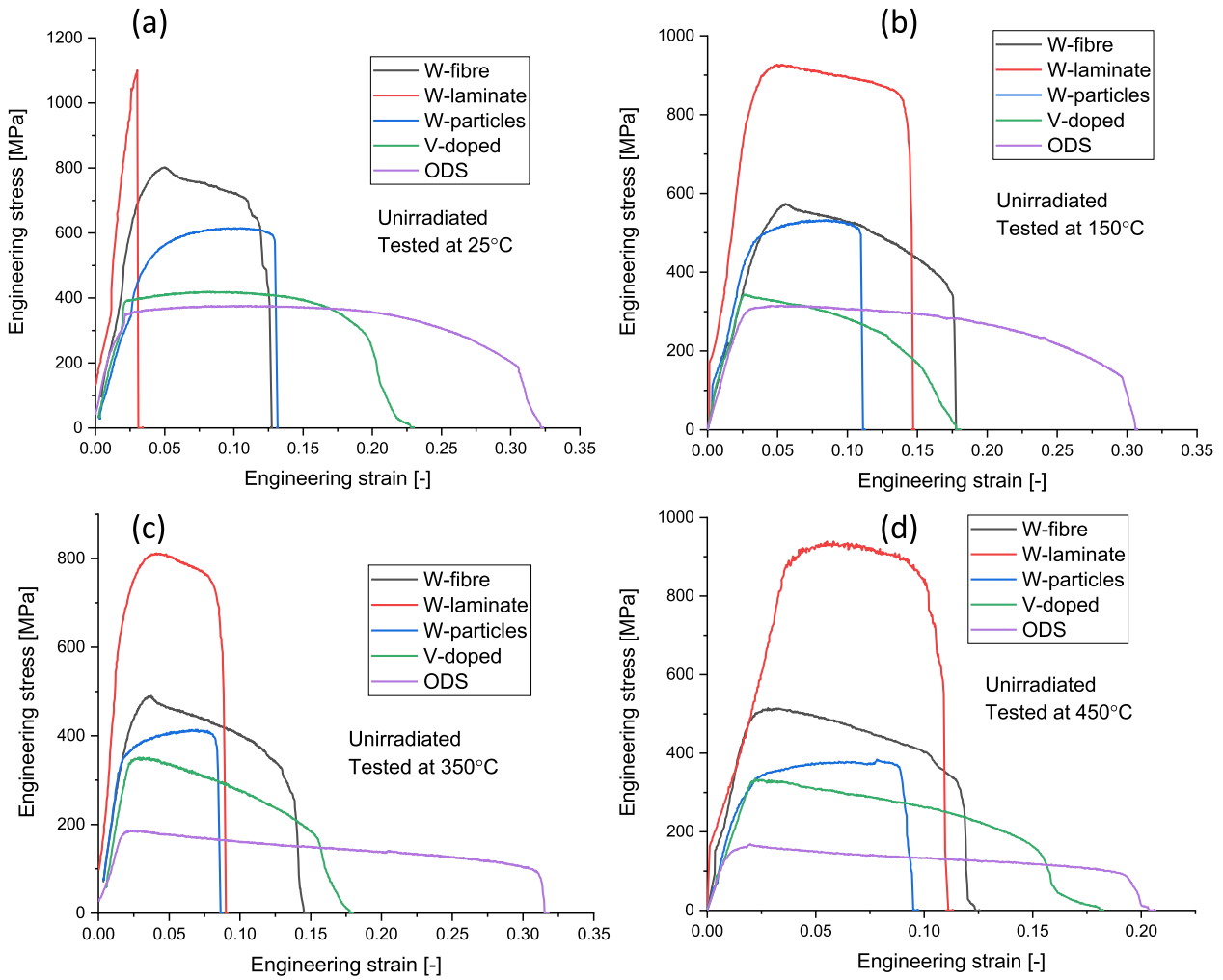


Fig. 19. Stress-strain data on non-irradiated materials obtained at (a) 25 °C, (b) 150 °C, (c) 350 °C and (d) 450 °C.

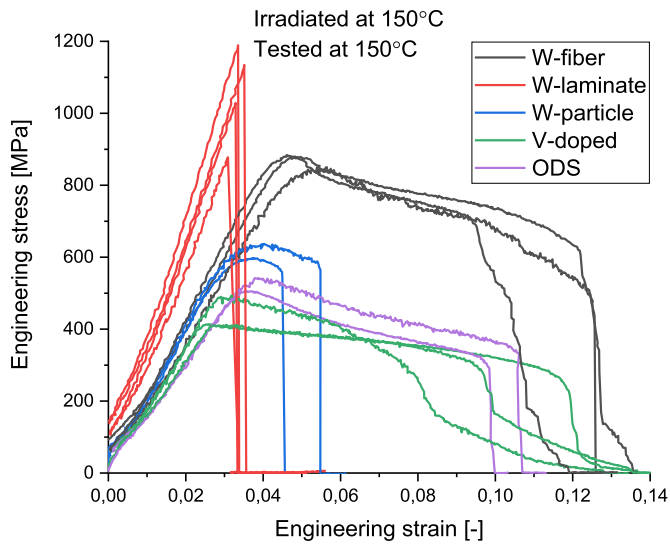


Fig. 20. Stress-strain data on the materials irradiated and tested at 150 °C.

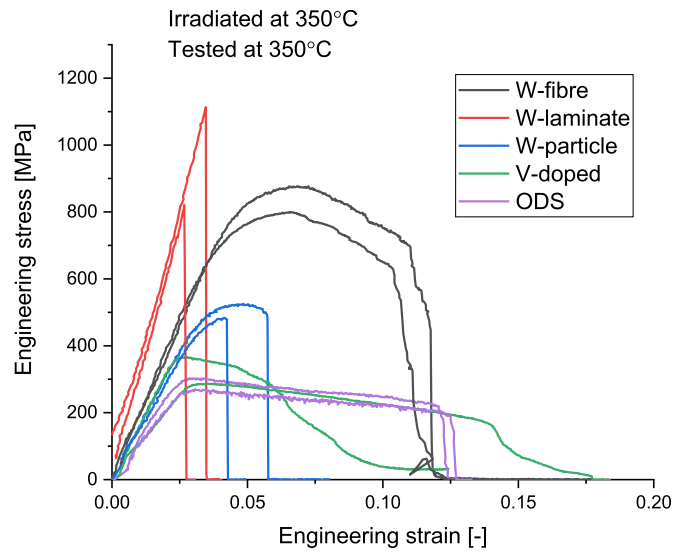


Fig. 21. Stress-strain data on the materials irradiated and tested at 350 °C.

stress are presented in Annex 2.

For the V-doped material tested at RT, the fracture stress and fracture strain after irradiation at 150 °C increase just slightly above the

reference value. At  $T_{irr} = T_{test} = 150\text{ °C}$ , we found a significant spread of the fracture strain and fracture stress. By comparing the average value from three tests, both the fracture stress and fracture strain in as-



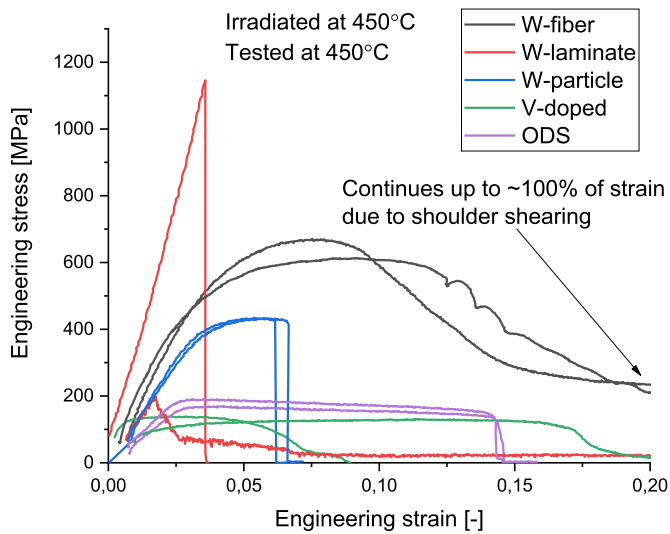


Fig. 22. Stress-strain data on the materials irradiated and tested at 450 °C.

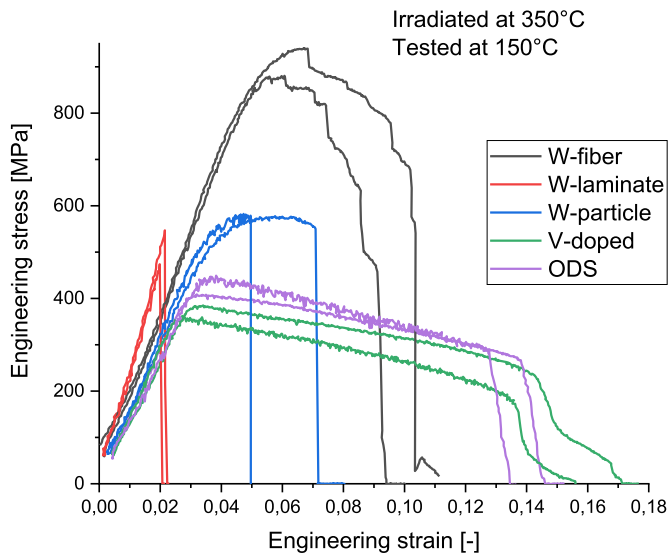


Fig. 23. Stress-strain data on the materials irradiated at 350 °C and tested at 150 °C.

irradiated state are reduced compared to the reference values. At  $T_{irr}$  350 and 450 °C, the fracture strain exhibits strong reduction, while the fracture stress increases after  $T_{irr}$  350 °C and reduces below the reference value after  $T_{irr}$  450 °C.

In the ODS material the fracture strain is essentially reduced in all the irradiated samples compared to the reference ones. The fracture stress of the ODS material irradiated at 150 °C is reduced at  $T_{test}$  RT and  $T_{irr}$   $T_{test}$  150 °C, while the specimens irradiated and tested at  $T_{irr}$   $T_{test}$  350 and 450 °C show an increase of the fracture stress compared to the reference value.

It is found that for any irradiation and test temperature, the ductility of the V-doped grade is better i.e. a larger or a similar fracture strain for  $T_{irr}$  450 °C and  $T_{test}$  450 °C. Besides that, the fracture stress of the irradiated V-doped grade is systematically larger than that of irradiated ODS grades, when the test temperature is below the irradiation temperature (except for tests at RT after  $T_{irr}$  150 °C), while no clear trend is established for the case of  $T_{irr}$   $T_{test}$ .

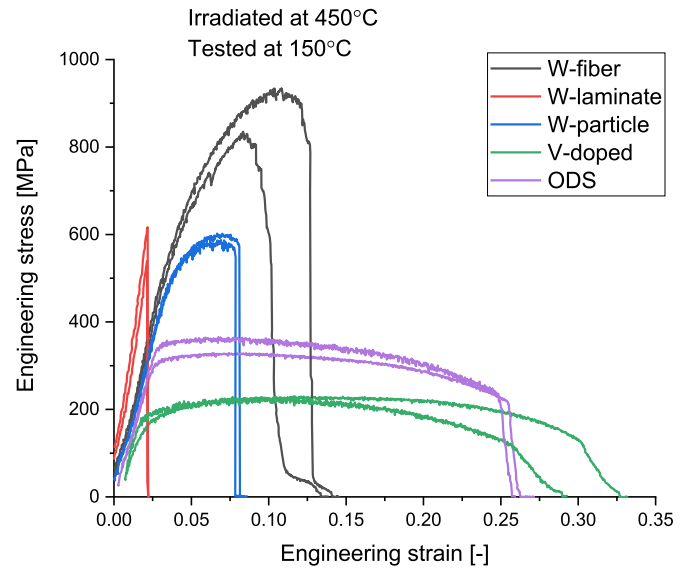


Fig. 24. Stress-strain data on the materials irradiated at 450 °C and tested at 150 °C.

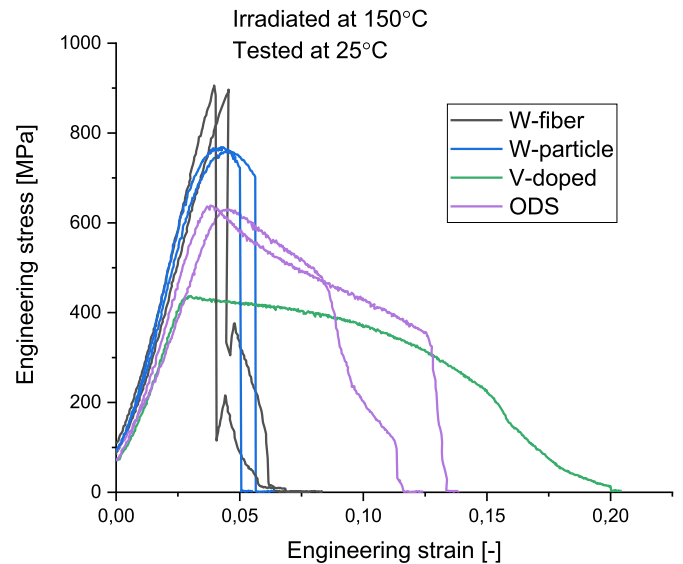


Fig. 25. Stress-strain data on the materials irradiated at 150 °C and tested at RT.

#### 4. Discussion

The effect of the neutron irradiation has been studied in a series of advanced Cu-based alloys and composites specially developed for the application in the temperature range of 150–450 °C as structural material in a nuclear fusion environment. This study tested several Cu-based alloys with different strengthening elements i.e. W-fiber, W-laminate, W-particle, ODS particles and V-Cr-Zr precipitates. Even in the non-irradiated state, due to the different principle of strengthening, the deformation and failure behavior was governed by various mechanisms. Following the microstructural analysis, it is possible to say that the failure in the W-fiber and W-laminate composites was directly controlled by the mechanical strength of the corresponding armoring elements. In the ODS and V-doped materials, the failure was controlled by the classical ductile post-necking deformation, formation of void damage, void coalescence and eventual dimple rupture. W-particle reinforced copper showed extended hardening stage with rather high uniform elongation

**Table 3**

Mapping of the samples in the irradiation capsules depending on floor and position on the floor. Schematics of the irradiation capsule with location of the floors and positions is shown in Fig. 17. The labels in the table have the following correspondence: *V* = V-doped, *P* = W-particle, *L* = W-laminate, *F* = W-fiber, *Y* – ODS.

	Position 1	Position 2	Position 3	Position 4	Position 5	Position 6	Position 7
Level 1	V	P	L	F	Y	L	Y
Level 2	V	P	F	F	F	L	Y
Level 3	V	P	V	F	P	L	Y

**Table 4**

Tensile data for non-irradiated specimens.

Condition: Unirradiated						
Material: V-doped						
Test temperature ( °C)	Test specimen ID	Engineering yield stress (MPa)	Engineering UTS (MPa)	Uniform elongation, %	True fracture strain	True fracture stress (MPa)
25	V19	392	419	6.0	1.631	214
150	V1	342	344	0.2	2.228	319
300	V13	310	315	2.8		
350	V5	337	352	1.3	1.612	176
450	V6	331	336	0.3	1.728	189
Material: ODS						
25	Y2	352	377	9.5	1.735	1084
150	Y1	295	315	2.9	1.636	682
300	Y15	186	200	1.6	0.662	187
350	Y4	180	187	0.7	0.679	157
450	Y14	147	169	1.3	0.504	147

**Table 5**

Tensile data for specimens irradiated at  $T = 150$  °C.

Condition: Irradiated up to 2.5 dpa in Cu at 150 °C. Capsule TT1						
Material: V-doped						
Test temperature ( °C)	Test specimen ID	Yield stress (MPa)	UTS (MPa)	Uniform elongation,%	Fracture strain	Fracture stress (MPa)
25	V21	433	437	0.3	1.783	260
150	V16	428	431	0.2	0.077	47
150	V17	481	493	0.3	0.661	96
150	V20	408	412	0.7	0.980	110
150	average	439	445	0.4	0.573	84
Material: ODS						
25	Y19	614	631	0.4		
25	Y20	622	639	0.4	0.759	754
25	average	618	635	0.4	0.759	754
150	Y17	520	522	0.3	0.379	468
150	Y18	533	542	0.2		
150	average	527	532	0.3	0.379	468

**Table 6**

Tensile data for specimens irradiated at  $T = 350$  °C.

Condition: Irradiated up to 2.5 dpa in Cu at 350 °C. Capsule TT2						
Material: V-doped						
Test temperature ( °C)	Test specimen ID	Yield stress (MPa)	UTS (MPa)	Uniform elongation,%	Fracture strain	Fracture stress (MPa)
150	V12	375	379	0.4	1.065	649
150	V18	354	362	0.3	1.091	499
150	average	365	371	0.4	1.078	574
350	V7	361	366	0.2	0.115	124
350	V11	282	287	0.7	0.888	384
350	average	322	327	0.5	0.502	254
Material: ODS						
150	Y21	398	403	0.3	0.721	544
150	Y22	435	449	0.4		
150	average	417	426	0.4	0.721	544
350	Y9	292	314	0.6	0.241	293
350	Y10	256	268	0.4		
350	average	274	291	0.5	0.241	293

but much reduced total elongation if compared with ODS and V-doped materials. This difference can be explained by the accumulation of the stress contraction around W particles and reduced material's toughness

once the plastic damage emerges.”

As expected, the irradiation in the low-temperature range has caused significant hardening or even complete embrittlement of certain tested

**Table 7**Tensile data for specimens irradiated at  $T = 450$  °C.

Condition: Irradiated up to 2.5 dpa in Cu at 450 °C. Capsule TT3						
Material: V-doped						
Test temperature (°C)	Test specimen ID	Yield stress (MPa)	UTS (MPa)	Uniform elongation, %	Fracture strain	Fracture stress (MPa)
150	V22	176	229	7.8	1.945	752
150	V15	171	230	9.7	1.638	591
150	average	174	230	8.8	1.792	672
450	V8	151	158	2.0	0.383	82
450	V9	97	131	9.6	0.261	127
450	average	124	145	5.8	0.322	105
Material: ODS						
150	Y11	303	329	4.7	0.695	432
150	Y12	343	365	4.1		
150	average	323	347	4.4	0.695	432
450	Y7	167	176	1.4		
450	Y8	184	190	0.5	0.320	195
450	average	176	183	1.0	0.320	195

materials. At high irradiation temperature, either softening or hardening could realize depending on the material. Some of the acquired stress-strain curves exhibit serrations, while some of the curves are smooth. The presence or lack of these serrations is not linked with the test methodology, as all tests were performed on the same equipment and with the same acquisition settings. In the case of non-irradiated samples, small amplitude serrations were observed only on the composite samples. After the irradiation, large amplitude serrations appeared only the W-fiber samples, which we attribute to the stress relaxation possibly related to the sliding of W fibers. Some small-amplitude serrations observed in the post-necking deformation of other samples (e.g. ODS, V-doped) could be explained by specifics of the plastic deformation after irradiation, namely: the formation of clear channels and large deformation bands (see discussion of these mechanisms in [40]). The small serrations during the work hardening stage could also originate from the dragging of the irradiation defects under elastic interaction of the dislocations, as computational studies performed in FCC and BCC metals suggest [41–44]. However, an in-depth discussion of the deformation mechanisms is out of the scope of this work as it requires detailed microstructural analysis engaging transmission electron microscopy.

Based on the presented results above, a number of preliminary conclusions on the effect of neutron irradiation up to 2.5 dpa on the mechanical properties and related damage mechanisms can be made for each studied material. To facilitate listing the summary, Fig. 16 provides a synthesis of the results indicating the effect of the irradiation on the studied materials. In particular, Fig. 16(a-b) compares the absolute values of UTS before and after irradiation, while Fig. 16(c) provides the relative change of the UTS and Fig. 16(d) shows the absolute value of the uniform elongation after irradiation. The available literature data for the ITER-specification CuCrZr in two heat treatment conditions are added in Fig. 16a, b and c (detailed review of these results is presented in Section 2). As it can be seen from Fig. 16b, in the non-irradiated state the UTS of ITER-specification grades is comparable to V-doped and W-particle alloys studied here. After the irradiation, softening occurs in the SACwA CuCrZr at  $T_{irr} = T_{test} = 350$  °C. Only one of the materials studied here demonstrated irradiation softening at  $T_{irr} = T_{test} = 350$  °C – a decrease by 35 MPa in the V-doped CuCrZr.

Below, we summarize the main findings related to the irradiation effect on the tensile characteristics and morphology of the fracture surface for each tested grade separately.

The uniform elongation is reduced to zero (i.e. fully brittle) at each irradiation temperature and at each investigated test condition. Moreover, after irradiation at 450 °C, the ultimate tensile stress becomes lower than in the non-irradiated state.

The fracture after irradiation occurs by the rupture of tungsten foils by intergranular fracture. Large cracks are observed near W-Cu interfaces. This observation indicates that either the W foil or the W/Cu

interface represents a weak spot. Given that the irradiation effect on the plasticity of W constituents should be similar in W-fiber, W-laminate and W-particle, the origin of the embrittlement of W-laminate material is unlikely solely related to the damage accumulated in the laminate tungsten. The incurred embrittlement could be related to the irradiation-induced diffusion occurring near the W/Cu interfaces, which suppresses the ductility otherwise present in the non-irradiated state. Detailed TEM investigation and localized chemical analysis is required to clarify the reason. Another possible reason for the embrittlement can be the formation of Re/Os clusters and/or non-coherent precipitates and/or segregation zones inside of W laminates. However, we must note that the irradiation temperature of 150–300 °C was not high enough for the long-range vacancy diffusion in tungsten material, as the vacancy migration occurs above 400 °C [45]. Therefore, unless the Re/Os solutes can be efficiently transported by self-interstitial defects, the transmuted solutes should stay dissolved. Further micro-chemical investigation by atom probe would provide an answer to this question.

The uniform elongation is reduced down to 1–5% compared to 5% in the non-irradiated state. The irradiation hardening yielded to 300–350 MPa at  $T_{irr} = 150$  and 350 °C, and considerably lower value of 100 MPa at  $T_{irr} = 450$  °C. Hence, the accumulation of the damage in this material is strongly affected by the increase of the irradiation temperature from 350 to 450 °C.

The fracture occurs by ductile deformation of the Cu matrix and necking of W-fibers. At RT, fully brittle fracture of tungsten fibers is observed. At  $T_{irr} = T_{test} = 150$  °C, the fracture surface of W fibers resembles those in the non-irradiated state. However, the area reduction of individual fibers is reduced compared with the non-irradiated samples.

The irradiation leads to the reduction of the uniform elongation down to 1–2% compared to 6–10% in the non-irradiated state. This reduction occurs irrespective of the irradiation temperature.

Irradiation hardening has reached 50 MPa (at  $T_{irr} = 450$  °C) and 100 MPa ( $T_{irr} = 150$  and 350 °C), which can be considered as limited (i.e. non-significant) effect, given that in the ITER specification CuCrZr the saturated irradiation hardening is about 300 MPa.

The fracture occurs by ductile deformation of the Cu matrix irrespective of irradiation/test condition. Shear or debonding of W particles is observed depending on their size such that large particles are sheared, small ones are debonded. This finding indicates that the irradiation provokes stress concentration near large W particles leading to subsequent shear deformation and thereby initiating fast crack propagation. Overall, this might have consequences for the reduction of the fracture toughness and reduced fatigue endurance.

The uniform elongation is reduced from 0.7 to 9.5% in the non-irradiated state down to 0.5–1% irrespective of the irradiation temperature. Despite very small uniform elongation in the irradiated state, the post necking deformation yields to the total elongation reaching 23% or

the true fracture strain reaching 0.76. The irradiation hardening, on the other hand, strongly depends on the irradiation temperature. The hardening decreases as nearly 200 → 100 → 0 MPa as  $T_{\text{irr}}$  increases from 150 up to 450 °C. This may indicate that ODS particles are more effective recombination sites for the irradiation defects at higher temperatures.

The fracture occurs by ductile deformation by dimples and shear at 150 and 350 °C. Intensive oxidation is found in tests performed at 450 °C, which obstructs the observation of the dimples.

The uniform elongation of this material increases up to 9% after the irradiation at 450 °C, while before the irradiation it is only 0.5% at test temperature of 450 °C. The improvement of the uniform elongation is accompanied by softening (i.e. reduction of UTS). At the lower irradiation temperatures, the uniform elongation is reduced down to 0.5% followed by a considerable post-necking deformation (in a similar way observed for ITER specification CuCrZr), however the irradiation hardening is rather limited being 100 MPa at  $T_{\text{irr}}$  150 °C.

The fracture occurs by the ductile deformation ended with the dimple rupture and shear, irrespective of the test and irradiation temperature.

## 5. Conclusions

To conclude, we summarize the most important findings with respect to the observed irradiation effects in the studied materials and provide assessment of the two aspects of the irradiation damage addressed in this study, namely: (i) low temperature embrittlement and (ii) high temperature softening.

The sign of the low temperature embrittlement (at  $T_{\text{irr}}$   $T_{\text{test}}$  150 °C) which is usually expressed as the increase of yield stress and drastic reduction of the uniform and total elongation has been observed in all studied materials but at different extent. In the case of W-laminates, the irradiation led to the fully brittle failure, while for the V-doped and ODS materials the embrittlement is limited to the disappearance of the uniform elongation retaining a considerable post-necking deformation. The W-particle material sustained limited uniform elongation with a moderate irradiation hardening. W-fiber material experienced hardening but yet did not lose the ability for small uniform elongation and considerable post necking deformation, importantly the fracture surface of the tungsten fibers demonstrated signs of plastic deformation and necking.

At the side of the high irradiation and test temperature (i.e.  $T_{\text{irr}}$   $T_{\text{test}}$  450 °C), irradiation softening occurred in the V-doped material. In the V-doped and ODS materials the UTS dropped below 200 MPa. The W-laminate remains fully brittle. The W-particle and W-fiber materials did not get softer and kept sustaining limited uniform elongation.

The post-irradiation testing at  $T_{\text{irr}}$   $T_{\text{test}}$  450 °C has shown that yield stress in W-laminate and V-doped grades has dropped below the reference value i.e. softening occurred. In the case of the ODS material, no softening was found, but at  $T_{\text{irr}}$   $T_{\text{test}}$  450 °C, the UTS approaches the non-irradiated value. In the W-fiber and W-particle materials, no softening occurs at 450 °C. After the irradiation at 350 °C, no softening was registered in four out of five tested materials, and merely a slight softening was registered in the V-doped material, which is certainly a positive outcome. With this result, one may further need to explore the irradiation creep and cyclic fatigue endurance, since as of now, the irradiation creep above 300 °C [46] as well as fatigue life after the irradiation at 250–350 °C [47,48,49] are posing an essential problem.

In the previous studies, the decrease in size of the  $\text{Al}_2\text{O}_3$  particles (in GlidCop Al25, which is an analogous of  $\text{Cu-Y}_2\text{O}_3$  studied here) was registered under the irradiation at 180 °C by 3 MeV ions [50], the reduction of particle size at 300 °C was also observed. This particle size reduction is probably linked with ballistic mixing, and therefore could be a dose-dependent degradation process. Hence, the particle stability at larger irradiation doses such as those expected for DEMO (10–15 dpa) requires further validation.

Another interesting point to note is the absolute value of the irradiation hardening. According to the available literature review, performed by Zinkle et al. [51], saturation of the irradiation hardening in copper at  $T_{\text{irr}}$  20–200 °C occurs around 0.1–1 dpa, and the resulting value is around 250–300 MPa. In the present study, at least at low irradiation temperature, one should expect the saturation of the irradiation damage as well (except the continuous transmutation of Re/Os in W-containing composites). The obtained results show that the irradiation hardening at 150 °C yields to 100–300 MPa, where the maximum is reached in W-fiber material. Hence, we see that within the explored neutron fluence, the severity of the irradiation hardening is comparable or even lower than in copper.

From the view point of the ductility reduction, limited information obtained for Cu and CuCrZr alloys [51] suggest that the uniform elongation reaches zero at the irradiation doses of 0.1–1 dpa, depending on the irradiation temperature. As has been measured in the present study, the uniform elongation is reduced down to 0.5–9% in all materials (except W-laminates which are fully brittle), however, the post necking deformation remains significant for the ODS and V-doped grades. At the same time, both of these grades exhibit much lower YS and UTS compared with the W-particle and W-fiber materials.

## Annex 1 experimental details

The tensile samples have a flat-type dog bone geometry with a total length of 16 mm and the dimensions of the grip section is a width of 4.2 mm and a thickness of 1 mm. The gage length is 5.2 mm and the gage cross-section is  $1 \times 1.5 \text{ mm}^2$ . The irradiation capsules were made of stainless steel and the tensile samples were placed inside a metallic holder. The holders were made of aluminum for the irradiation temperature of 150 °C, and titanium for the irradiation temperature of 350 and 450 °C. Each capsule had three vertical positions (hereafter “levels”) on which 21 samples (seven pieces per level) were placed. In such a way, for each irradiation temperature, four samples of each material plus one spare (W-fiber material) were irradiated. The mapping of the sample location in the capsules is shown in Table 3 and in Fig. 17.

To evaluate the fracture stress, the cross-section area  $A$  was measured by SEM and calculated from the resulting cross-section micrographs using the software ImageJ [31] as presented in Appendix B in Supplementary Material. As presented in Appendix A of supplementary material, the load at fracture was identified from load-displacement curves, where either an abrupt decrease of load was observed (marked by blue arrow) or 10% of the ultimate tensile strength value was reached (if no blue arrow is shown), if such an abrupt decrease of load was not identified (following the guideline of ASTM E8/E8M-21).

The qualitative and quantitative analyses of the microstructures of the fracture surfaces were carried out with the ImageJ software applied on the scanning electron microscopy (SEM) images at appropriate magnifications. To make the SEM analysis, the broken half pieces of the tensile samples were investigated by SEM. Prior to the SEM in hot cell, the samples were cleaned in the ultra-sonic bath. All SEM images presented in this work were acquired using a secondary electron (SE) detector. The employed scanning electron microscope was a JEOL JSM-7100LV (JEOL, Tokyo, Japan) and the operating conditions were: 20 kV accelerating voltage and 12–20 mm working distance. The samples were loaded on the electric tray in a separate chamber as shown in Fig. 18 and then transferred inside the SEM in a neighbor chamber.

## Annex 2 stress-strain response

The reference (i.e. non-irradiated state) stress-strain curves are shown in Fig. 19.

Fig. 20 provides the stress-strain curves at  $T_{\text{irr}}$   $T_{\text{test}}$  150 °C.

Fig. 21 provides the stress-strain curves at  $T_{\text{irr}}$   $T_{\text{test}}$  350 °C.

Fig. 22 provides the stress-strain curves at  $T_{\text{irr}}$   $T_{\text{test}}$  450 °C.

Fig. 23 and Fig. 24 provide the stress-strain data obtained at

$T_{\text{test}} = 150\text{ }^{\circ}\text{C}$ , while the irradiation temperature was  $350\text{ }^{\circ}\text{C}$  and  $450\text{ }^{\circ}\text{C}$ , respectively.

Fig. 25 provide the stress-strain curves obtained after the tests at RT and  $T_{\text{irr}} = 150\text{ }^{\circ}\text{C}$ .

### Annex 3 fracture strain and fracture stress

Tables 4–7 summarize values of the true strain after fracture (calculated with the help of Eq. (3) from the cross-section area, extracted from the SEM images) and true fracture stress for tensile tests in non-irradiated condition and irradiated at 150, 350 and  $450\text{ }^{\circ}\text{C}$ , respectively. The true fracture stress, reported in those tables, is calculated as the load at fracture divided by the fracture area measured by SEM. The SEM images with the selected area reduction and corresponding stress-strain curves are provided as Supplementary Material for this publication.

The fracture properties in gray and italic were extracted from the stress-strain curves, for which no clear fracture point could be identified (such as an inflection or a sudden drop of stress). In this case, the accuracy of the extracted data is limited since the fracture point was identified conventionally as 10% of UTS value following the guideline of ASTM E8/E8M-21. Because of such identification, in some cases of extensive post-necking deformation (in the non-irradiated state), the fracture stress turns out to be lower than the UTS.

### CRediT authorship contribution statement

**Dmitry Terentyev:** Conceptualization, Methodology, Software, Investigation, Writing – original draft, Writing – review & editing, Project administration, Funding acquisition. **Michael Rieth:** Writing – review & editing, Project administration, Funding acquisition. **Gerald Pintsuk:** Writing – review & editing, Project administration, Funding acquisition. **Alexander Von Müller:** Investigation, Writing – review & editing. **Steffen Antusch:** Writing – review & editing. **Aleksandr Zinovev:** Investigation, Writing – review & editing. **Alexander Bakaev:** Investigation, Writing – review & editing. **Kateryna Poleshchuk:** Investigation, Writing – review & editing. **Giacomo Aiello:** Writing – review & editing, Project administration, Funding acquisition.

### Declaration of Competing Interest

The authors declare that they have no known competing financial interests or personal relationships that could have appeared to influence the work reported in this paper.

### Acknowledgement

This work has been carried out within the framework of the EUROfusion Consortium and has received funding from the Euratom research and training program 2014–2018 and 2019–2020 under grant agreement No 633053. This work has been carried out within the framework of the EUROfusion Consortium, funded by the European Union via the Euratom Research and Training Programme (Grant Agreement No 101052200 — EUROfusion). Views and opinions expressed are however those of the author(s) only and do not necessarily reflect those of the European Union or the European Commission. Neither the European Union nor the European Commission can be held responsible for them.

### Supplementary materials

Supplementary material associated with this article can be found, in the online version, at doi:10.1016/j.jnucmat.2023.154587.

### References

- [1] G. Pintsuk, E. Diegele, S.L. Dudarev, M. Gorley, J. Henry, J. Reiser, M. Rieth, European materials development: results and perspective, *Fusion Eng. Des.* 146 (2019) 1300–1307.
- [2] J. Davis, V. Barabash, A. Makhankov, L. Ploch, K. Slattery, Assessment of tungsten for use in the ITER plasma facing components, *J. Nucl. Mater.* 258 (1998) 308–312.
- [3] S. Zinkle, N. Ghoniem, Operating temperature windows for fusion reactor structural materials, *Fusion Eng. Des.* 51 (2000) 55–71.
- [4] V. Barabash, G. Federici, M. Rodig, L. Snead, C. Wu, Neutron irradiation effects on plasma facing materials, *J. Nucl. Mater.* 283 (2000) 138–146.
- [5] D. Terentyev, G. De Temmerman, T.W. Morgan, Y. Zayachuk, K. Lambrinou, B. Minov, A. Dubinko, K. Bystrov, G. Van Oost, Effect of plastic deformation on deuterium retention and release in tungsten, *J. Appl. Phys.* 117 (8) (2015), 083302.
- [6] J. You, E. Visca, T. Barrett, B. Boswirth, F. Crescenzi, F. Dompail, M. Fursdon, F. Gallay, B. Ghidersa, H. Greuner, European divertor target concepts for DEMO: design rationales and high heat flux performance, *Nucl. Mater. Energy* 16 (2018) 1–11.
- [7] V.R. Barabash, G.M. Kalinin, S.A. Fabritsiev, S.J. Zinkle, Specification of CuCrZr alloy properties after various thermo-mechanical treatments and design allowables including neutron irradiation effects, *J. Nucl. Mater.* 417 (1–3) (2011) 904–907.
- [8] D. Maisonnier, D. Campbell, I. Cook, L. Di Pace, L. Giancarli, J. Hayward, A. L. Puma, M. Medrano, P. Norajitra, M. Rocella, P. Sardain, M.Q. Tran, D. Ward, Power plant conceptual studies in Europe, *Nucl. Fusion.* 47 (11) (2007) 1524–1532.
- [9] S. Noce, G. Dose, D. Flammini, V. Imbriani, G. Mazzone, F. Moro, S. Roccella, F. Romanelli, R. Villari, E. Visca, J.H. You, Nuclear analyses for the design of the ITER-like plasma facing components vertical targets of the DEMO divertor, *Fusion Eng. Des.* 155 (2020).
- [10] S.A. Fabritsiev, A.S. Pokrovsky, Effect of high doses of neutron irradiation on physico-mechanical properties of copper alloys for ITER applications, *Fusion Eng. Des.* 73 (1) (2005) 19–34.
- [11] G. Federici, W. Biel, M.R. Gilbert, R. Kemp, N. Taylor, R. Wenninger, European DEMO design strategy and consequences for materials, *Nucl. Fusion.* 57 (9) (2017).
- [12] S.A. Fabritsiev, A.S. Pokrovsky, Effect of irradiation temperature on microstructure, radiation hardening and embrittlement of pure copper and copper-based alloy, *J. Nucl. Mater.* 367 (2007) 977–983.
- [13] B. Singh, D. Edwards, P. Toft, Effect of neutron irradiation and post-irradiation annealing on microstructure and mechanical properties of OFHC-copper, *J. Nucl. Mater.* 299 (2001) 205–218.
- [14] A. Gusarov, C. Pohl, T. Pfalz, R.W. Bosch, S. Van Dyck, V. Barabash, R. Eaton, F. Zaccchia, H. Samuli, Assessment of creep in reactor-irradiated CuCrZr alloy intended for the ITER first wall panels, *Fusion Eng. Des.* 137 (2018) 112–123.
- [15] O. Gillia, L. Briottet, I. Chu, P. Lemoine, E. Rigal, A. Peacock, Characterization of CuCrZr and CuCrZr/SS joint strength for different blanket components manufacturing conditions, *J. Nucl. Mater.* (2009) 830–833, 386–88.
- [16] G. Piatti, D. Boerman, Hot tensile characteristics and microstructure of a Cu-0.65Cr-0.08Zr alloy for fusion-reactor applications, *J. Nucl. Mater.* 185 (1) (1991) 29–38.
- [17] B. Singh, S. Golubov, H. Trinkaus, A. Serra, Y. Osetsky, A. Barashev, Aspects of microstructure evolution under cascade damage conditions, *J. Nucl. Mater.* 251 (1997) 107–122.
- [18] J. Reiser, L. Garrison, H. Greuner, J. Hoffmann, T. Weingartner, U. Jantsch, M. Klimenkov, P. Franke, S. Bonk, C. Bonnekoh, S. Sicking, S. Baumgartner, D. Bolich, M. Hoffmann, R. Ziegler, J. Konrad, J. Hohe, A. Hoffmann, T. Mrotzek, M. Seiss, M. Rieth, A. Moslang, Ductilisation of tungsten (W): tungsten laminated composites, *Int. J. Refract. Met. H* 69 (2017) 66–109.
- [19] J. Reiser, M. Rieth, A. Moslang, B. Dafferner, A. Hoffmann, X.O. Yi, D.E. J. Armstrong, Tungsten foil laminate for structural divertor applications - Tensile test properties of tungsten foil, *J. Nucl. Mater.* 434 (1–3) (2013) 357–366.
- [20] A.V. Müller, B. Boswirth, V. Cerri, H. Greuner, R. Neu, U. Siefken, E. Visca, J. H. You, Application of tungsten-copper composite heat sink materials to plasma-facing component mock-ups, *Phys. Scr.* T171 (1) (2020).
- [21] A. Von Müller, D. Ewert, A. Galatanu, M. Milwich, R. Neu, J.Y. Pastor, U. Siefken, E. Tejado, J.H. You, Melt infiltrated tungsten-copper composites as advanced heat sink materials for plasma facing components of future nuclear fusion devices, *Fusion Eng. Des.* 124 (2017) 455–459.
- [22] J.W. Coenen, Y. Mao, S. Sistla, A.V. Müller, G. Pintsuk, M. Wirtz, J. Riesch, T. Hoeschen, A. Terra, J.H. You, H. Greuner, A. Kreter, C. Broeckmann, R. Neu, C. Linsmeier, Materials development for new high heat-flux component mock-ups for DEMO, *Fusion Eng. Des.* 146 (2019) 1431–1436.
- [23] J.H. You, A. Brendel, S. Nawka, T. Schubert, B. Kieback, Thermal and mechanical properties of infiltrated W/CuCrZr composite materials for functionally graded heat sink application, *J. Nucl. Mater.* 438 (1–3) (2013) 1–6.
- [24] D. Pelowitz, J. Durkee, J. Elson, M. Fensin, M. James, R. Johns, G. McKinney, S. Mashnik, L. Waters, T. Wilcox, MCNPX 2.7. 0 Extensions, Los Alamos National Laboratory, 2011.
- [25] A. Stankovskiy, G. Van den Eynde, L. Fiorito, ALEPH V.2.7, A Monte Carlo Burn-Up Code, SCK CEN, 2018.
- [26] A. Plompen, et al., JEFF-3.3, Nuclear Energy Agency, 2017.
- [27] D.A. Brown, M. Chadwick, R. Capote, A. Kahler, A. Trkov, M. Herman, A. Sonzogni, Y. Danon, A. Carlson, M. Dunn, ENDF/B-VIII. 0: the 8th major release of the nuclear reaction data library with CIELO-project cross sections, new standards and thermal scattering data, *Nucl. Data Sheets* 148 (2018) 1–142.
- [28] A.Y. Konobeyev, U. Fischer, Y.A. Korovin, S. Simakov, Evaluation of effective threshold displacement energies and other data required for the calculation of



- advanced atomic displacement cross-sections, *Nucl. Energy Technol.* 3 (3) (2017) 169–175.
- [29] M. Norgett, M. Robinson, I. Torrens, A proposed method of calculating displacement dose rates, *Nucl. Eng. Des.* 33 (1) (1975) 50–54.
- [30] J.M. Choung, S.R. Cho, Study on true stress correction from tensile tests, *J. Mech. Sci. Technol.* 22 (6) (2008) 1039–1051.
- [31] C.A. Schneider, W.S. Rasband, K.W. Eliceiri, NIH Image to ImageJ: 25 years of image analysis, *Nat. Methods* 9 (7) (2012) 671–675.
- [32] S.K. Lee, H.C. Hsu, W.H. Tuan, Oxidation behavior of copper at a temperature below 300 °C and the methodology for passivation, *Mater. Res.-Ibero-Am. J.* 19 (1) (2016) 51–56.
- [33] J. Reiser, J. Hoffmann, U. Jantsch, M. Klimenkov, S. Bonk, C. Bonnekoh, A. Hoffmann, T. Mrotzek, M. Rieth, Ductilisation of tungsten (W): on the increase of strength AND room-temperature tensile ductility through cold-rolling, *Int. J. Refract. Met. H* 64 (2017) 261–278.
- [34] D. Terentyev, J. Riesch, S. Lebedev, A. Bakaeva, J.W. Coenen, Mechanical properties of as-fabricated and 2300 °C annealed tungsten wire tested up to 600 °C, *Int. J. Refract. Met. H* 66 (2017) 127–134.
- [35] G. Kalinin, V. Barabash, A. Cardella, J. Dietz, K. Ioki, R. Matera, R.T. Santoro, R. Tivey, I.H. Teams, Assessment and selection of materials for ITER in-vessel components, *J. Nucl. Mater.* 283 (2000) 10–19.
- [36] K. Zhang, Evaluate and initiate developments of CuCrZr materials property handbook, KIT, Eurofus. Rep. IDM Ref. 2NRCT (2018).
- [37] L.M. Garrison, Y. Katoh, L.L. Snead, T.S. Byun, J. Reiser, M. Rieth, Irradiation effects in tungsten-copper laminate composite, *J. Nucl. Mater.* 481 (2016) 134–146.
- [38] A. Zinovev, D. Terentyev, C.C. Chang, C. Yin, A. Bakaev, M. Rieth, P. Lied, J. Reiser, C. Bonnekoh, Effect of neutron irradiation on ductility of tungsten foils developed for tungsten-copper laminates, *Nucl. Mater. Energy* 30 (2022).
- [39] D. Terentyev, W. Van Renterghem, L. Tanure, A. Dubinko, J. Riesch, S. Lebediev, T. Khvan, K. Verbeken, J.W. Coenen, E.E. Zhurkin, Correlation of microstructural and mechanical properties of K-doped tungsten fibers used as reinforcement of tungsten matrix for high temperature applications, *Int. J. Refract. Met. H* 79 (2019) 204–216.
- [40] B. Singh, N. Ghoniem, H. Trinkaus, Experiment-based modelling of hardening and localized plasticity in metals irradiated under cascade damage conditions, *J. Nucl. Mater.* 307–311 (2002) 159–170.
- [41] T. Nogaret, C. Robertson, D. Rodney, Atomic-scale plasticity in the presence of Frank loops, *Philos. Mag.* 87 (6) (2007) 945–966.
- [42] D. Terentyev, A. Bakaev, Y.N. Osetsky, Interaction of dislocations with Frank loops in Fe-Ni alloys and pure Ni: an MD study, *J. Nucl. Mater.* 442 (2013) 628–632.
- [43] D. Terentyev, G. Monnet, P. Grigorev, Transfer of molecular dynamics data to dislocation dynamics to assess dislocation–dislocation loop interaction in iron, *Scr. Mater.* 69 (2013) 578–581.
- [44] D.A. Terentyev, Y.N. Osetsky, D.J. Bacon, Effects of temperature on structure and mobility of the < 1 0 0 >-edge dislocation in body-centred cubic iron, *Acta Mater.* 58 (7) (2010) 2477–2482.
- [45] L.K. Keys, J.P. Smith, J. Motteff, High-temperature recovery of tungsten after neutron irradiation, *Phys. Rev.* 176 (1968) 851–856.
- [46] I.V. Gorynin, S.A. Fabritsiev, V.V. Rybin, V.A. Kasakov, A.S. Pokrovskii, V. R. Barabash, Y.G. Prokofiyev, Radiation-resistant properties of copper-alloys intended for fusion-reactor applications, *J. Nucl. Mater.* 191 (1992) 401–406.
- [47] B.N. Singh, J.F. Stubbins, P. Toft, The influence of neutron irradiation on the fatigue performance of OFHC copper and a dispersion strengthened copper alloy, *J. Nucl. Mater.* 275 (2) (1999) 125–137.
- [48] K.D. Leedy, J.F. Stubbins, B.N. Singh, F.A. Garner, Fatigue behavior of copper and selected copper alloys for high heat flux applications, *J. Nucl. Mater.* 233 (1996) 547–552.
- [49] T.S. Srivatsan, S. Anand, J.D. Troxell, High-strain cyclic fatigue and fracture of an oxide dispersion-strengthened copper alloy, *Eng. Fract. Mech.* 46 (2) (1993) 183–198.
- [50] S.J. Zinkle, E.V. Nesterova, V.R. Barabash, V.V. Rybin, A.V. Naberrenkov, Effect of ion irradiation on the structural stability of dispersion-strengthened copper-alloys, *J. Nucl. Mater.* 208 (1–2) (1994) 119–127.
- [51] M. Li, S.J. Zinkle, Radiation effects in copper and copper alloys for fusion applications, *Comprehens. Nucl. Mater.* 6 (2020) 93–113, 2nd edition.